AD-A109 717 SRI INTERNATIONAL MENLO PARK CA F/G 18/3
LABORATORY INVESTIGATION OF CONTAINMENT IN UNDERGROUND NUCLEAR --ETC(U)
FEB 81 J C CIZEK, A L FLORENCE DNA001-80-C-0040
UNCLASSIFIED DNA-5731F NL

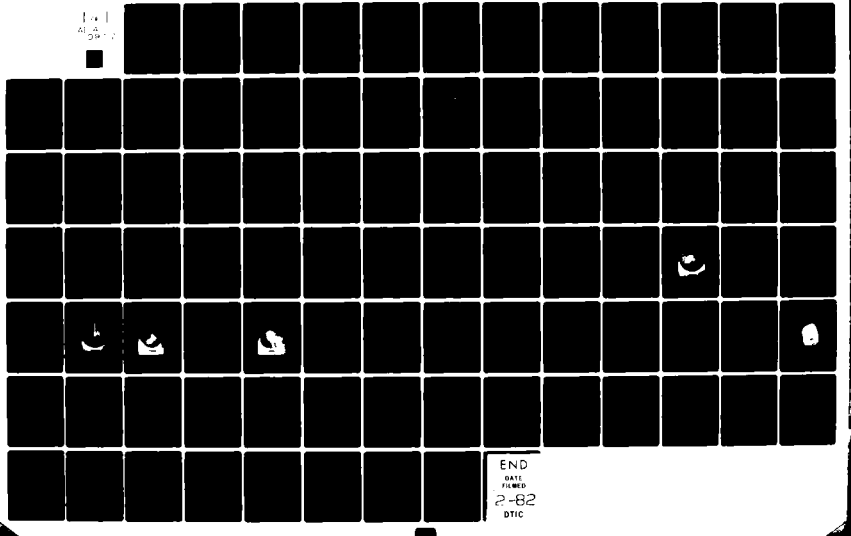

END
DATE FILMED
2-82
DTIC

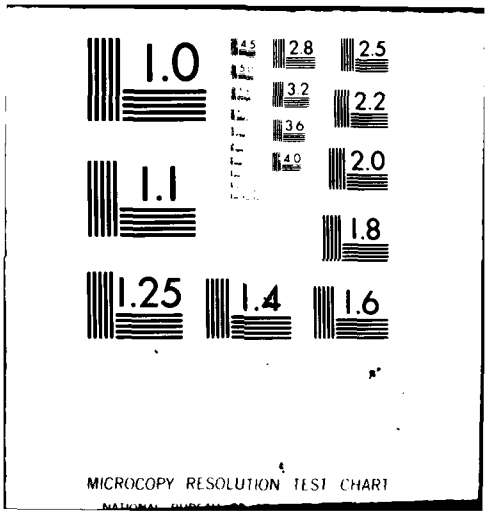
1.0
1.1
1.25
1.4
1.6
1.8
2.0
2.2
2.5
2.8
3.2
3.6
4.0
MICROCOPY RESOLUTION TEST CHART

DNA 5731F

LABORATORY INVESTIGATION OF CONTAINMENT IN UNDERGROUND NUCLEAR TESTS

J. C. Cizek
A. L. Florence
SRI International
333 Ravenswood Avenue
Menlo Park, California 94025

15 February 1981

Final Report for Period 17 December 1979—15 February 1981

CONTRACT No. DNA 001-80-C-0040

APPROVED FOR PUBLIC RELEASE;
DISTRIBUTION UNLIMITED.

THIS WORK SPONSORED BY THE DEFENSE NUCLEAR AGENCY
UNDER RDT&E RMSS CODE B345080462 J24AAXYX98373 H2590D.

Prepared for
Director
DEFENSE NUCLEAR AGENCY
Washington, D. C. 20305

Destroy this report when it is no longer needed. Do not return to sender.

PLEASE NOTIFY THE DEFENSE NUCLEAR AGENCY, ATTN: STTI, WASHINGTON, D.C. 20305, IF YOUR ADDRESS IS INCORRECT, IF YOU WISH TO BE DELETED FROM THE DISTRIBUTION LIST, OR IF THE ADDRESSEE IS NO LONGER EMPLOYED BY YOUR ORGANIZATION.

UNCLASSIFIED

SECURITY CLASSIFICATION OF THIS PAGE *(When Data Entered)*

REPORT DOCUMENTATION PAGE	READ INSTRUCTIONS BEFORE COMPLETING FORM
1. REPORT NUMBER: DNA 5731F	2. GOVT ACCESSION NO.: AD-A109 717
3. RECIPIENT'S CATALOG NUMBER:	
4. TITLE *(and Subtitle)*: LABORATORY INVESTIGATION OF CONTAINMENT IN UNDERGROUND NUCLEAR TESTS	5. TYPE OF REPORT & PERIOD COVERED: Final Report for Period 17 Dec 79 to 15 Feb 81
	6. PERFORMING ORG. REPORT NUMBER: SRI PYU-1289
7. AUTHOR(s): J. C. Cizek and A. L. Florence	8. CONTRACT OR GRANT NUMBER(s): DNA 001-80-C-0040
9. PERFORMING ORGANIZATION NAME AND ADDRESS: SRI International, 333 Ravenswood Avenue, Menlo Park, CA 94025	10. PROGRAM ELEMENT, PROJECT, TASK AREA & WORK UNIT NUMBERS: Subtask J24AAXYX983-73
11. CONTROLLING OFFICE NAME AND ADDRESS: Director, Defense Nuclear Agency, Washington, D.C. 20305	12. REPORT DATE: 15 February 1981
	13. NUMBER OF PAGES: 90
14. MONITORING AGENCY NAME & ADDRESS*(if different from Controlling Office)*:	15. SECURITY CLASS *(of this report)*: UNCLASSIFIED
	15a. DECLASSIFICATION/DOWNGRADING SCHEDULE: N/A

16. DISTRIBUTION STATEMENT *(of this Report)*

Approved for public release; distribution unlimited.

17. DISTRIBUTION STATEMENT *(of the abstract entered in Block 20, if different from Report)*

18. SUPPLEMENTARY NOTES

This work sponsored by the Defense Nuclear Agency under RDT&E RMSS Code B345080462 J24AAXYX98373 H2590D.

19. KEY WORDS *(Continue on reverse side if necessary and identify by block number)*

Nuclear	Cavity	Overburden
Underground	Hydrofracture	Uncoupled cavity
Explosion	Fracture initiation	Residual stress
Containment	Crack growth	Stress relaxation

20. ABSTRACT *(Continue on reverse side if necessary and identify by block number)*

In support of the overall DNA program for stemming and containment of underground nuclear tests, existing laboratory techniques were further developed and applied to investigate the effects of a dynamically generated residual stress field on the containment of gases in exploded-device cavities. Laboratory experiments were performed on externally pressurized grout spheres containing a small explosive charge cast at the center. Immediately after detonation, water is pumped into the exploded cavity at a constant flow rate

DD FORM 1 JAN 73 1473 EDITION OF 1 NOV 65 IS OBSOLETE

UNCLASSIFIED

SECURITY CLASSIFICATION OF THIS PAGE *(When Data Entered)*

20. ABSTRACT (Continued)

until the sphere is fractured to the outer surface. The fracture initiation pressures determined from the hydrofracture records are found to be substantially higher than those obtained in corresponding unexploded cavity experiments. This result provides a measure of the benefit to containment of the residual stress field created by the explosion.

Relaxation of the residual stress field was investigated by using a wide range of pumping rates, maintaining a constant cavity pressure for a time before hydrofracture, and by strain and stress gage measurements.

An attempt was made to obtain hydrofracture records for uncoupled exploded cavities (air space around the charge). Although not successful, it was found that only a minor modification to the technique is required to provide the results.

PREFACE

This research was conducted under Contract DNA001-80-C-0040 in support of the DNA stemming and containment program for underground nuclear tests.

The authors are indebted to the technical monitor, Carl Keller (FCDNA), for technical ideas, suggestions, and overall guidance, and to the containment participants at Systems, Science and Software and Pacifica Technology for the insights provided by their theoretical work and critical commentaries.

The authors are also indebted to the personnel at SRI International who contributed directly to the research program. In particular, appreciation is extended to D. D. Keough for guidance in the development of embedded sensors, to G. R. Greenfield and T. J. Henry for the design and fabrication of instrumentation, to L. J. Dary for preparing the models and suggesting improvements, and to G. R. Abrahamson for overall supervision.

CONVERSION FACTORS

To Convert From	To	Multiple By
atmosphere (normal)	kilo pascal (kPa)	1.013 25 X E +2
bar	kilo pascal (kPa)	1.000 000 X E +2
foot	meter (m)	3.048 000 X E -1
inch	meter (m)	2.540 000 X E -2
mil	meter (m)	2.540 000 X E -5
ounce	kilogram (kg)	2.834 952 X E -2
poise	kilogram/meter-second (kg/m•sec)	1.000 000 X E -1
pound-force (lbf avoirdupois)	newton (N)	4.448 222
pound-force/inch^2 (psi)	kilo pascal (kPa)	6.894 757
pound-mass (lbm avoirdupois)	kilogram (kg)	4.535 924 X E -1

TABLE OF CONTENTS

TABLE OF CONTENTS (continued)

LIST OF ILLUSTRATIONS

LIST OF ILLUSTRATIONS (continued)

LIST OF ILLUSTRATIONS (continued)

LIST OF TABLES

SECTION 1
INTRODUCTION AND SUMMARY

1.1 INTRODUCTION

A requirement of underground nuclear testing is that radioactive gases be prevented from entering the atmosphere. In general, this requirement will be met if experimental tunnels leading from the nuclear device cavity are stemmed successfully and if the cavity gases are contained by the adjacent surrounding medium. A residual stress field is generated in this surrounding medium by the explosion and probably aids containment. Although containment has been achieved for many years and stemming has generally been successful in recent nuclear tests, the complexities associated with geological and test-site features require that planned tests still receive extensive containment evaluation.

Over the years, the DNA stemming and containment (SAC) program has consisted of five main parts: code development for ground motion, tunnel closure, and grout flow calculations; material properties determination; laboratory investigations; scaled high explosive tests; and field diagnostics. Over the past several years SRI has been conducting laboratory investigations.[1-7]

Our laboratory investigations during the last year have focused on containment. One purpose of the experimental program has been to compare the containment capability of cavities generated under a variety of conditions. Another purpose is to validate calculations[8-10] of the residual stress field as a major containment feature of underground nuclear tests. The data generated in the laboratory are suitable for correlation with the predictions of existing codes. The experimental technique has also been used to determine the influence of major geological and test site features. Although our basic containment experiment may not be regarded as a small-scale version of an explosively simulated underground nuclear test, simulation is close enough to provide the correct important mechanisms required in a study of containment.

In our basic containment experiment, a small spherical charge is cast at the center of a sphere of rock-matching grout (RMG) with properties similar to those of Nevada Test Site tuff. The RMG sphere is hydraulically pressurized to represent overburden. The explosive is detonated, and dyed fluid is immediately pumped into the cavity at a constant flow rate until a fracture is propagated to the surface of the sphere and a steady radial pressure gradient is established. (In an alternative version of this test, residual cavity gases are vented before the start of hydrofracture.) The internal pressure is removed, and then the external pressure is removed. The cracked sphere is drained and tapped into two parts with a chisel, and the exposed fracture surfaces are photographed. The effect of the explosively generated residual stress field on containment is assessed by conducting a separate hydrofracture test on a sphere with an unexploded cavity comparable in size to the exploded cavity.

Series of exploded and unexploded cavity hydrofracture tests were performed on RMG spheres of 12-inch (30.48-cm) diameter to establish the effects of parameter variations on the basic containment experiment. In the standard exploded cavity test, a 3/8-gram charge of PETN* generated a 0.808-inch (2.05-cm) diameter cavity, which was unvented. In unexploded cavity tests, a smooth and unlined cavity having a 3/4-inch (1.90-cm)-diameter cavity was cast. The fixed parameters were overburden pressure [1000 psi (6.895 MPa)] and viscosity of the hydrofracture fluid (1 centipoise). The rate of fluid flow into the cavity varied. Surface gages monitored fracture arrival. Gages are continually under development to allow us to monitor residual stress and strain formation and relaxation. The specific areas of investigation were as follows:

- Influence on containment of time between detonation and hydrofracture. Dyed water was pumped into unexploded and exploded cavities at constant rates of 40.8, 61.2, and 122.4 cm^3/min.

*Pentaerythritol tetranitrate ($C_5H_8O_{12}N_4$).

- Stress relaxation. Hydrofracture experiments, in which the cavity pressure was held constant for 10 seconds following charge detonation, were performed on unvented exploded cavity spheres.
- Strain measurements. Strain decay due to stress relaxation in unvented exploded cavity spheres was monitored. The static strain associated with hydrofracture of unexploded cavity spheres was also measured.
- Uncoupled cavity. Attempts were made to perform hydrofracture tests on unvented exploded cavities having initial cavity diameters 1.5 and 3 times the charge diameter.
- Vented cavity. Cavity gases were released from exploded cavity spheres before hydrofracture and gasfracture tests.
- Stress measurements. Ytterbium and flat jack stress gages were improved and applied in an attempt to monitor residual stress formation and decay near an exploded cavity.

In addition, reproducibility of the 3/8-gram explosive source was assessed by monitoring the pressure pulse generated in the overburden fluid during exploded cavity tests. Particle velocity measurements obtained in an independent laboratory program provided additional data for verifying the calculations.

The tests performed during the current phase of the laboratory program are tabulated according to category in Section 3.1. Section 2 describes the most recent experimental developments, and Section 3 presents and discusses the hydrofracture results. Appendix A examines the cooling of cavity gases in a sealed exploded cavity as well as the pressurizing of an unvented exploded cavity during hydrofracture. Appendix B describes material properties for rock-matching grout RMG 2C4, the grout used in all the experiments.

1.2 SUMMARY

The principal findings of the above investigations were as follows:

- Flow rates over a wide range have negligible effect on fracture initiation pressures of unexploded cavity spheres. Reproducibility of the hydrofracture records is good for each flow rate (Figure 3.1).

- Increasing the flow rate in unvented exploded cavity tests increases the maximum hydrofracture pressures by reducing cavity gas pressure decay and stress relaxation. Maximum hydrofracture pressures were nearly four times those generated in unexploded cavities. Reproducibility is good for each flow rate (Figures 3.4, 3.8, and 3.9).
- Strain gage measurements for hydrofracture of unexploded cavity spheres result in radial strains nearly twice the value predicted by elasticity theory (Figure 3.3).
- Stress relaxation occurring at constant cavity gas pressure reduces the subsequent hydrofracture pressures in unvented exploded cavity tests (Figure 3.10).
- Vented exploded cavity spheres yield a spectrum of hydrofracture pressures for a wide range of flow rates. Fracture initiation pressures are higher than those generated in unexploded cavity tests. Increasing the flow rate promotes stable crack growth following fracture initiation (Figure 3.12).
- Low hydrofracture pressures in vented and unvented exploded cavity spheres are associated with planar fracture surfaces (Figures 3.5 and 3.7). High pressures are associated with complex fracture patterns (Figures 3.6 and 3.13).
- Strain gage measurements of the residual strain near an unvented exploded cavity implies substantial stress relaxation during the scaled times of relevance for underground nuclear tests (Figures 3.15 and 3.16).
- The experimental technique for the uncoupled cavities probably allowed water to fill the space around the charge before detonation. A simple modification is suggested to correct the problem.

In conclusion, the residual stress field surrounding an explosively formed cavity enhances the containment capability of the cavity by increasing the subsequent hydrofracture pressures and stabilizing initial crack growth. A slow flow rate, low cavity gas pressure, and prolonged stress relaxation reduce the hydrofracture pressure in unvented exploded cavities.

Investigations during the next phase of the containment program will include:

- Further experimentation with uncoupled cavities using an improved technique.
- Additional high flow rate testing of unvented exploded cavities to determine the upper bound on hydrofracture pressure.

- Residual stress and strain measurements in exploded cavity spheres to determine the initial level of residual stress and the subsequent rate of decay.
- High flow rate testing of RMG and tuff cylinders to assess the influence of material properties on containment.
- Direct measurement of gas pressure in coupled and uncoupled exploded cavities.
- High flow rate hydrofracture testing of coupled and uncoupled exploded cavity spheres to determine the effects on containment of reduced overburden pressure and asymmetric overburden stress.

SECTION 2

EXPERIMENTAL DEVELOPMENT

2.1 CONCEPT

The experiment shown schematically in Figure 2.1 was devised[4] to simulate in the laboratory several relevant conditions associated with an underground nuclear test. A small spherical explosive charge representing the device is sealed in a thin Lucite container and cast in a much larger sphere of rock-matching grout (RMG) with properties similar to those of Nevada Test Site tuff [Figure 2.1(a)]. The grout sphere is cured and then hydraulically pressurized to represent overburden [Figure 2.1(b)]. The explosive is detonated and the residual gas pressure is measured [Figure 2.1(c)]. Fluid is immediately pumped into the cavity at a constant flow rate until fracture occurs and a steady flow develops along the fracture surface [Figure 2.1(d)]. An alternative version of this experiment was developed to allow hydrofracture following the venting of cavity gases. An alternative configuration was also developed to provide decoupling of the explosive charge from the surrounding material by means of an annular region of air.

The hydrofracture portion of the experiment is included to determine the effect of the residual stress field by comparing the cavity pressures required to crack the RMG sphere with and without residual stresses. In the experiments without a residual stress field, spherical cavities are cast in the grout sphere; these unexploded cavities are comparable in size to the fully coupled exploded cavities.

2.2 EXPERIMENTAL TECHNIQUES

Figure 2.2 shows the experimental apparatus. A 12-inch-diameter RMG sphere is shown inside a steel vessel containing oil or water that can be pressurized to the desired overburden. The sphere is suspended from the lid by a stainless steel tube cast in the grout. In a vented exploded

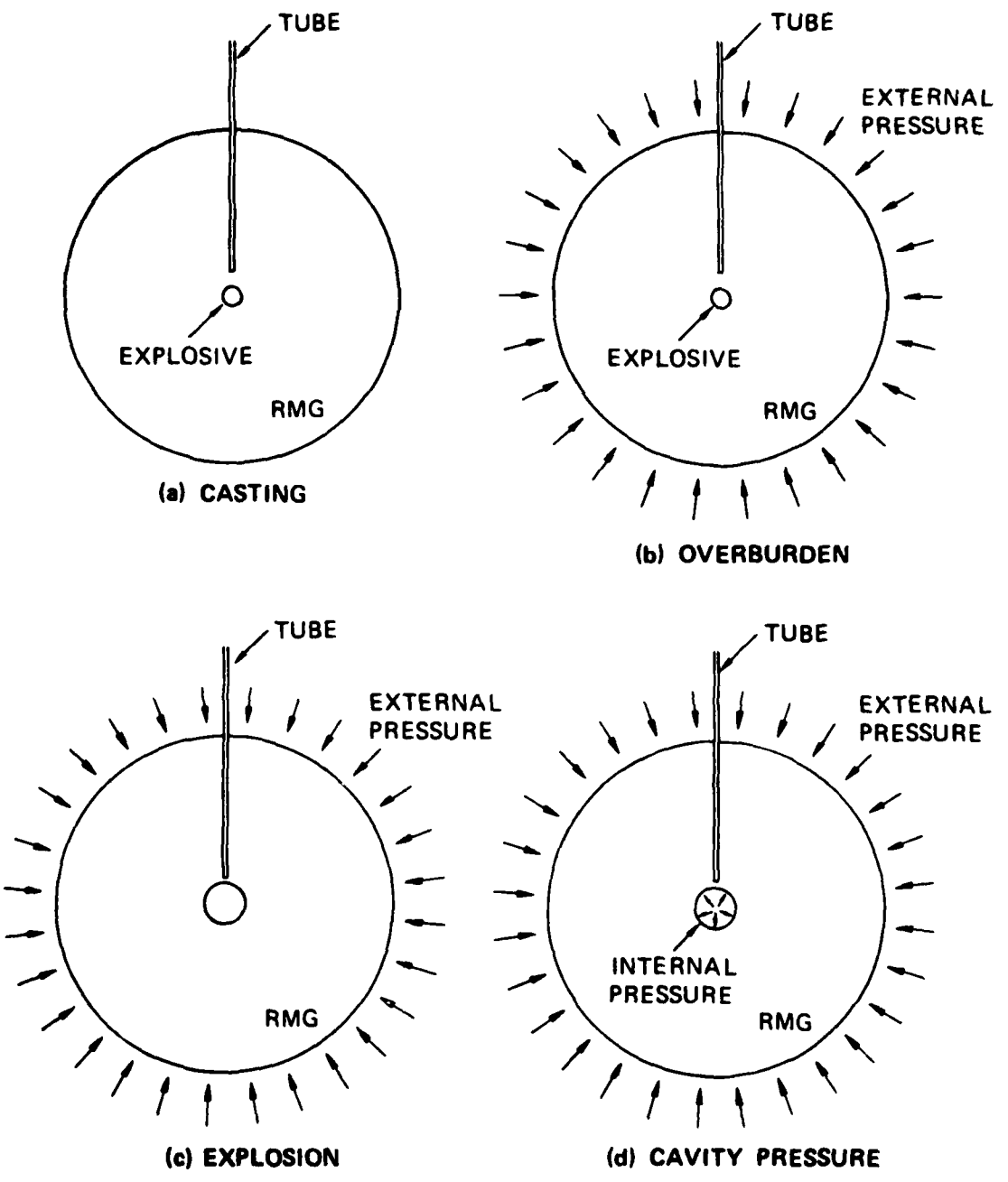

FIGURE 2.1 SEQUENCE OF OPERATIONS IN CONTAINMENT EXPERIMENTS
(Unvented Exploded Cavity)

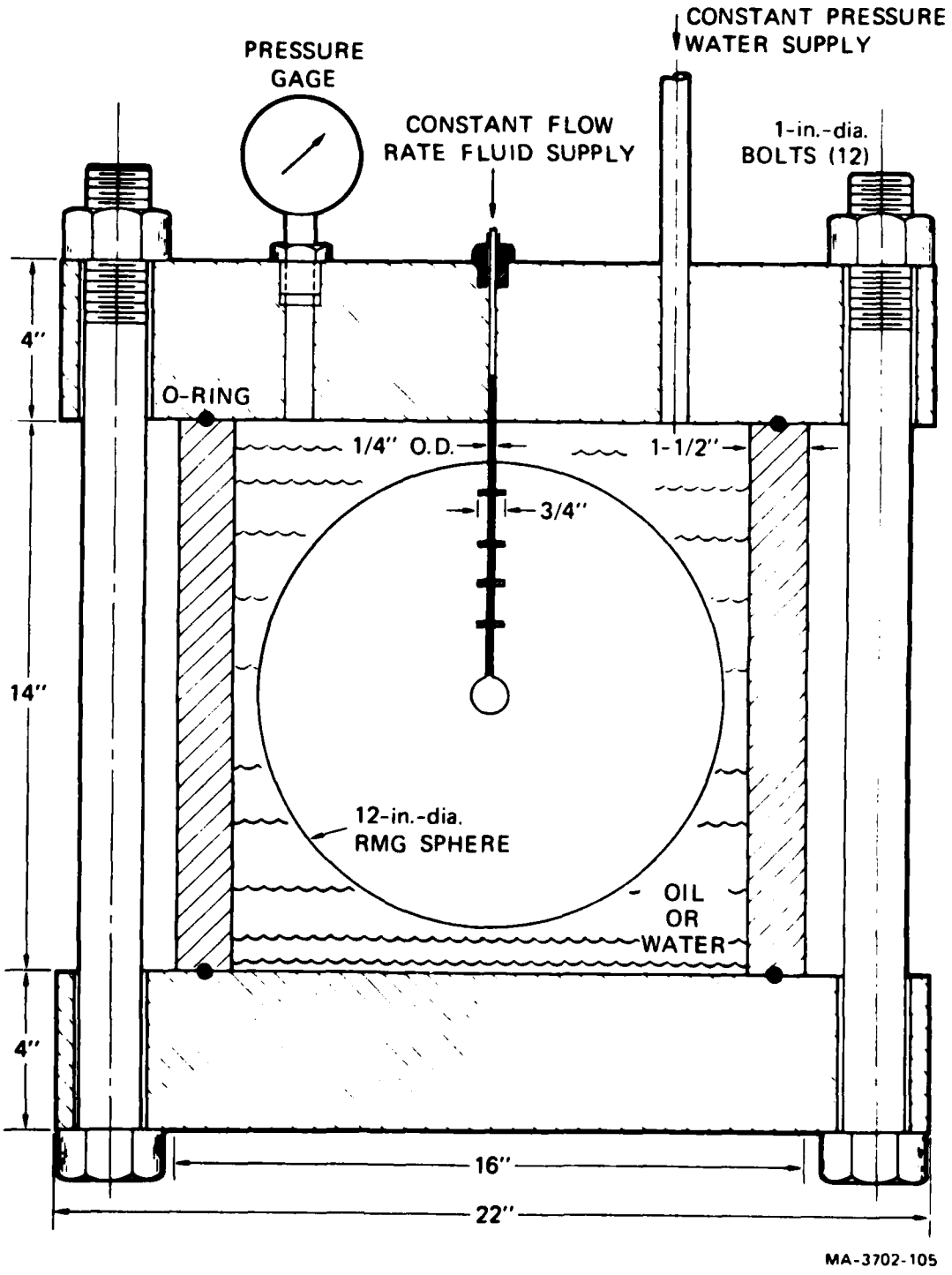

FIGURE 2.2 CONTAINMENT EXPERIMENT APPARATUS

cavity test, this tube provides a means for positioning the charge, potting in the detonator cables, and drilling into the cavity after detonation. The fluid in the vessel is maintained at a constant pressure throughout the test by incorporating a high-pressure nitrogen reservoir and valve in the water supply line. A quartz gage mounted in the bottom of the vessel monitors the pressure pulse generated by charge detonation.

The constant flow-rate system shown schematically in Figure 2.3 conforms with standard hydrofracture practice. The specifications of this system are as follows:

Motor:	Dayton Gear Motor Model 6K702C, 1.5 hp, 1740 rpm
Speed Reducers:	Winsmith Models 200 MWT (Ratio 5 to 1), 200 MWT (Ratio 10 to 1), M300T (Ratio 15 to 1)
Pump:	High Pressure Equipment Co. Model 62-6-10 30-cm^3 capacity, 10,000-psi maximum pressure (0.35-cm^3/revolution)
System:	Fluid: water dyed with Rhodamine B Volume (excluding pump): 42 cm^3

The motor shaft rotates at a constant angular velocity of 1740 rpm. Interchangeable speed reducers, with reduction ratios of 15 to 1, 10 to 1, and 5 to 1, provide shaft speeds of 116, 174, and 348 rpm, respectively. A slotted tubular coupling allows an extension of the shaft to translate as well as rotate. The shaft extension is threaded and rotates in a fixed threaded bearing, resulting in a constant velocity translation of the piston. The system provides constant pumping rates of 40.8, 61.2, and 122.4 cm^3/min into the cavity supply line (Figure 2.2).

Compliance of the hydrofracture system is measured by performing a pressure test in which the cavity is replaced by a rigid vessel of equivalent volume. The pressure-volume curve for this test is then used to compensate for the effects of system compliance on the hydrofracture records.

Details of the experimental techniques for unvented, vented, uncoupled, and unexploded cavity tests are given below.

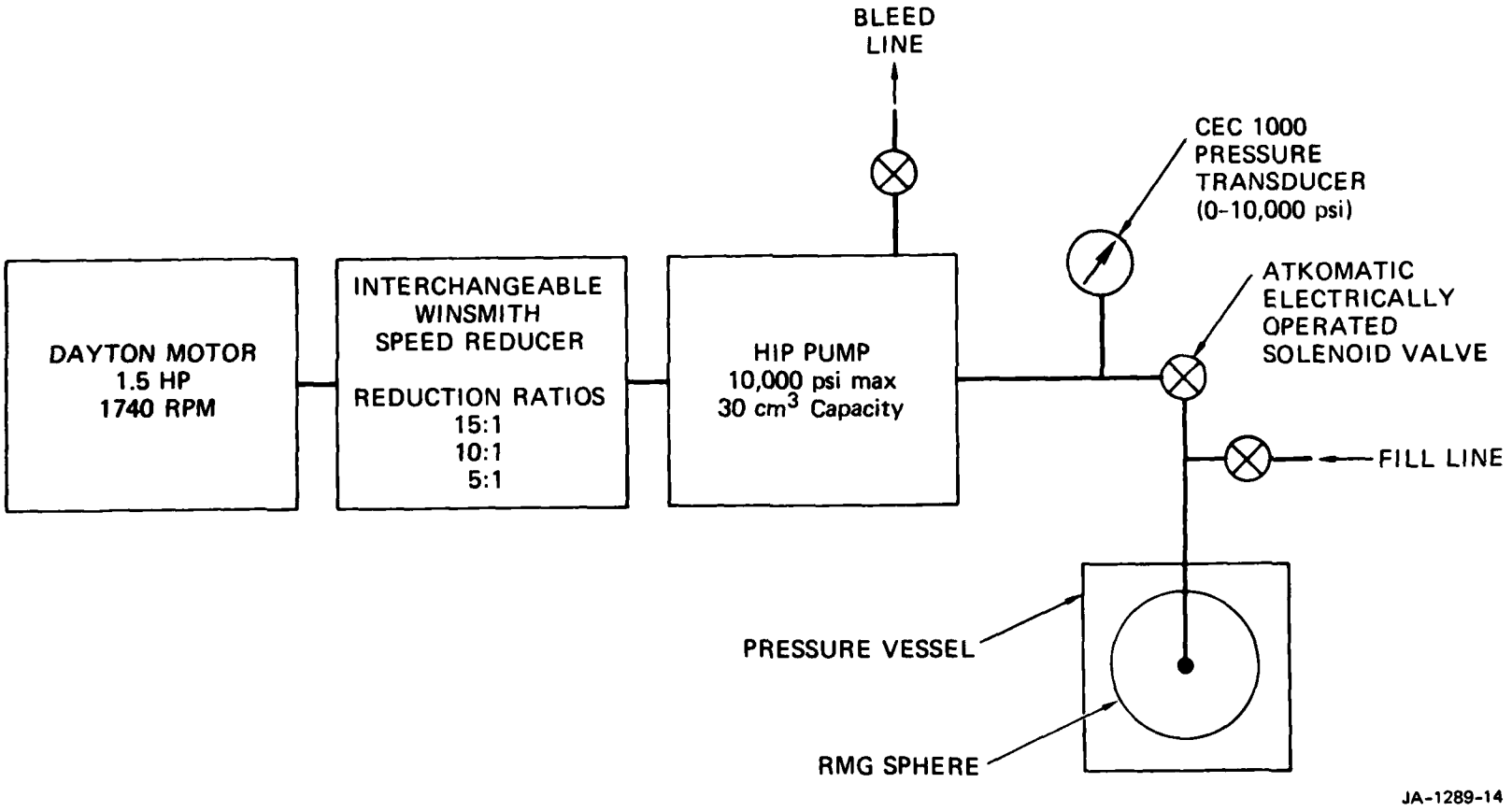

FIGURE 2.3 CONSTANT FLOW-RATE HYDROFRACTURE SYSTEM

Unvented Cavity Tests

The basic configuration for unvented exploded cavity hydrofracture tests is shown in Figure 2.4. Figure 2.5 shows the charge design, which consists of 3/8-gram of PETN in a 10-mm-OD Lucite case with a wall thickness of 20 mils (0.508 mm). A constant explosive density of 1 g/cm^3 was used for reproducibility; PETN weight varied slightly from charge to charge as a result of variations in machining accuracy. Hence, 3/8 gram was the nominal weight of the explosive. The charges were assembled by pressing PETN to a density of 1 g/cm^3 into a pair of mating Lucite hemispheres. The bridgewire assembly was then positioned as shown in Figure 2.5, using a notch in one of the hemispheres as a guide, and the hemispheres were snapped together and sealed with a 5 mil (0.127 mm) coating of Homalite.* Hence, the overall charge diameter was 0.404 in. (10.26 mm). A wide-angle ferrule was attached near the end of the access tube to compress the grout around the tube as the cavity expanded and prevented a leak path to the overburden from developing. The charge was positioned by gluing the charge holder to the steel ball that served as a valve during the test; the lead wires were brought out of the sphere along the plane of the equator.

Cavity gas pressure was measured and hydrofracture was performed by following the sequence of steps shown in Figure 2.6. Before charge detonation, the entire system was filled with hydrofracture fluid. The steel ball sealed the end of the access tube [Figure 2.6(a)]. Charge detonation expanded the cavity past the end of the tube [Figure 2.6(b)], and the ball valve opened the access tube [Figure 2.6(c)] when the cavity gas and hydrofracture fluid pressures reached equilibrium. These equilibrium pressures were measured by a pressure transducer located in the fluid supply line. Pumping began immediately with charge detonation. Hence the time required to open the access tube depended on the rates at which cavity gas pressure decayed and hydrofracture fluid was pressurized. This opening time may be reduced or eliminated by suitably prepressurizing the hydrofracture fluid.

*Homalite Corporation, Wilmington, Delaware.

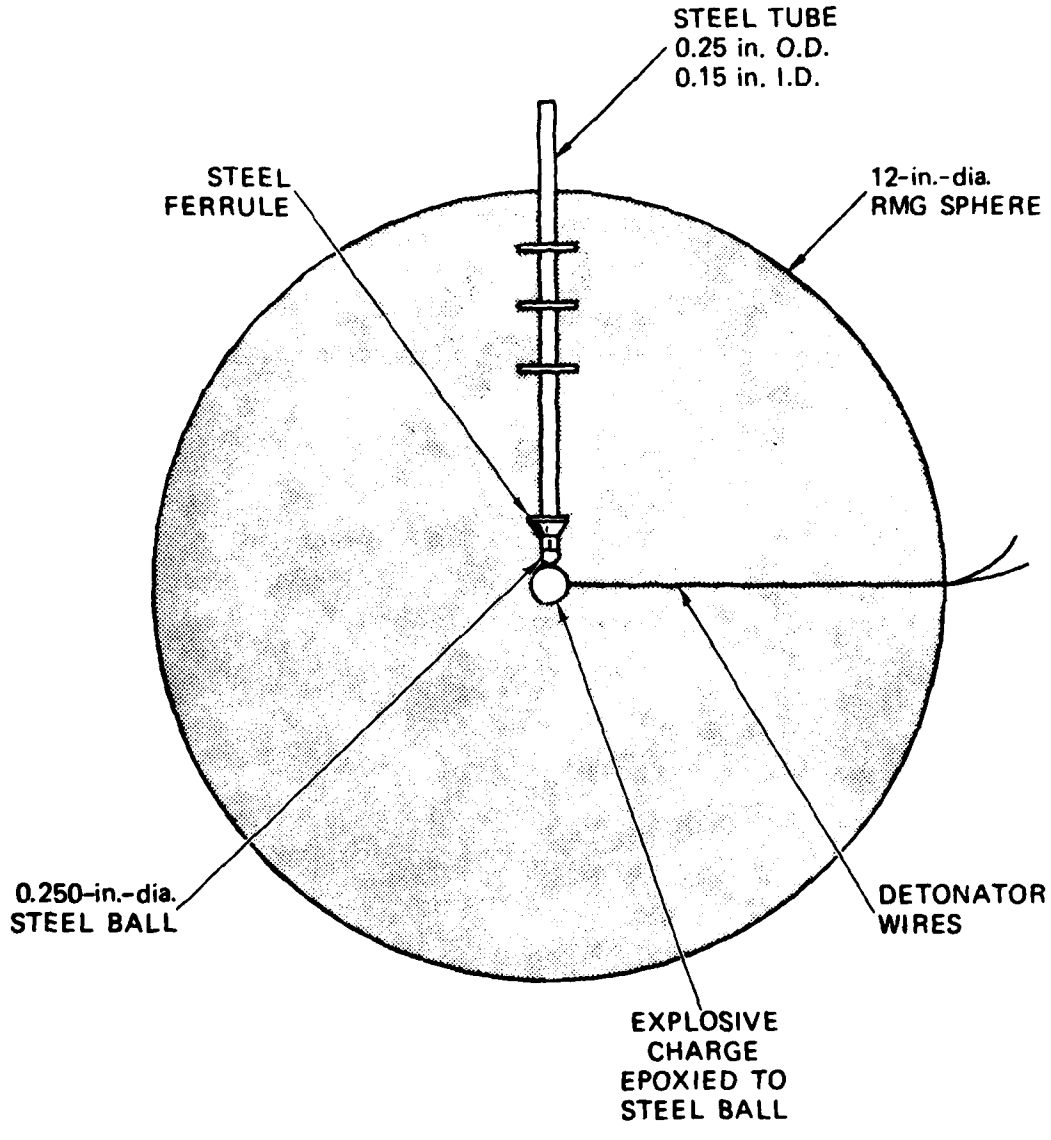

FIGURE 2.4 OVERALL CONFIGURATION FOR UNVENTED EXPLODED CAVITY TESTS

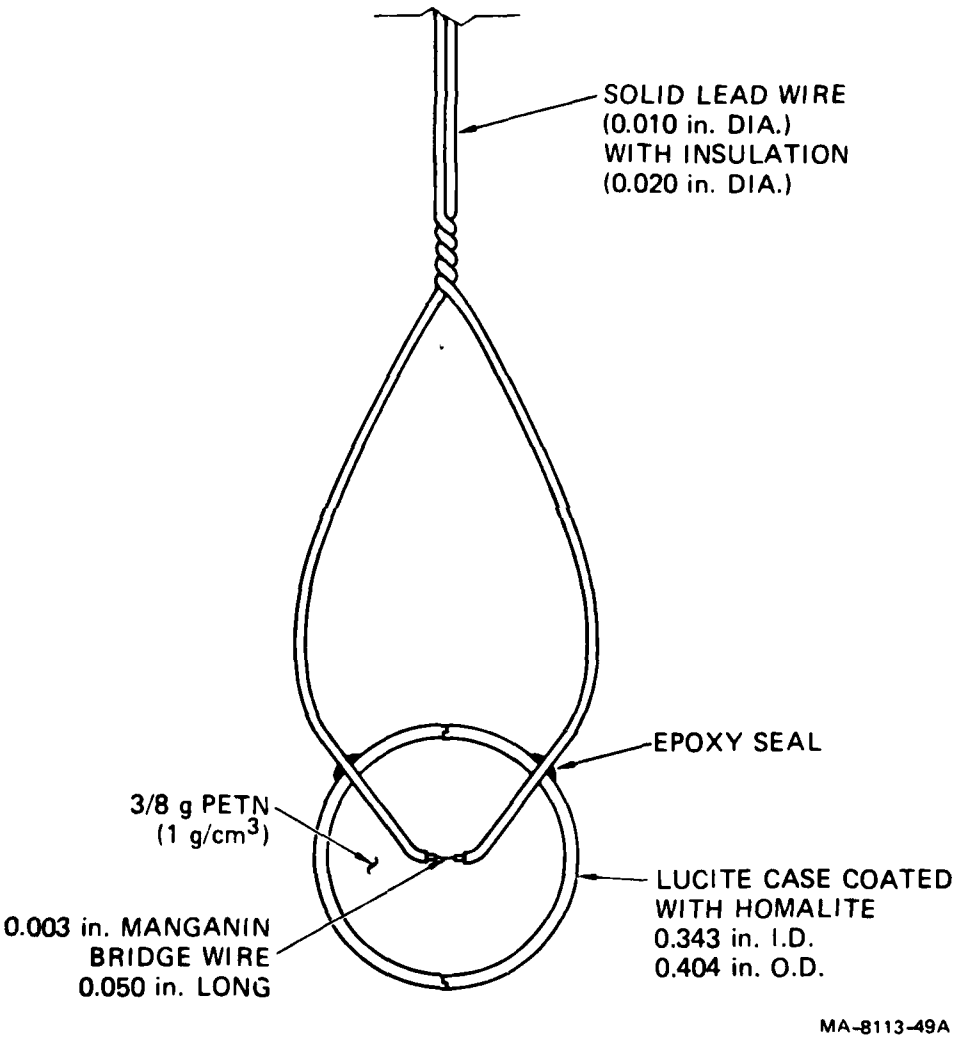

FIGURE 2.5 EXPLOSIVE CHARGE

Vented Cavity Tests

The basic configuration for vented exploded cavity hydrofracture tests is shown in Figure 2.7. The charge was positioned by drawing the lead wires through the access tube and filling the space between charge holder and tube with epoxy. The access tube was filled with epoxy. Venting occurred when the tube was drilled out following charge detonation. The drilling operation resulted in a 20-minute delay between charge detonation and hydrofracture. Hydrofracture pressures were measured by the pressure transducer located in the fluid supply line.

Uncoupled Cavity Tests

The basic configuration for uncoupled exploded cavity hydrofracture tests is shown in Figure 2.8. A thin-walled glass hemisphere with a 0.25-inch-diameter (0.635-cm) hole was Homalited to a washer on the access tube. A standard explosive charge was centered in the equatorial plane of the hemisphere and held in place by a plastic rod and Homalite. The rod was threaded into a steel ball that was Homalited to the end of the access tube. The lead wires from the charge were brought out through a notch in the glass, and a second glass hemisphere was Homalited in place to provide an annular region of air surrounding the charge. Rock-matching grout was poured around the glass sphere. The degree of uncoupling between the explosive source and surrounding grout was determined by the ratio of glass sphere diameter to charge diameter.

Unexploded Cavity Tests

The basic configuration for unexploded cavity hydrofracture tests is shown in Figure 2.9. The cavity was formed by first inserting a rubber membrane (balloon) through the access tube and expanding the tip with water to the desired diameter. A spherical shape was maintained by means of a wire cage, temporarily fastened to the end of the tube. After 48 hours, the membrane assumed a permanent shape and the cage was removed. The membrane and tube were then positioned in a Lucite mold and the grout was cast around them. After the grout cured, the membrane was removed, leaving a smooth unlined cavity.

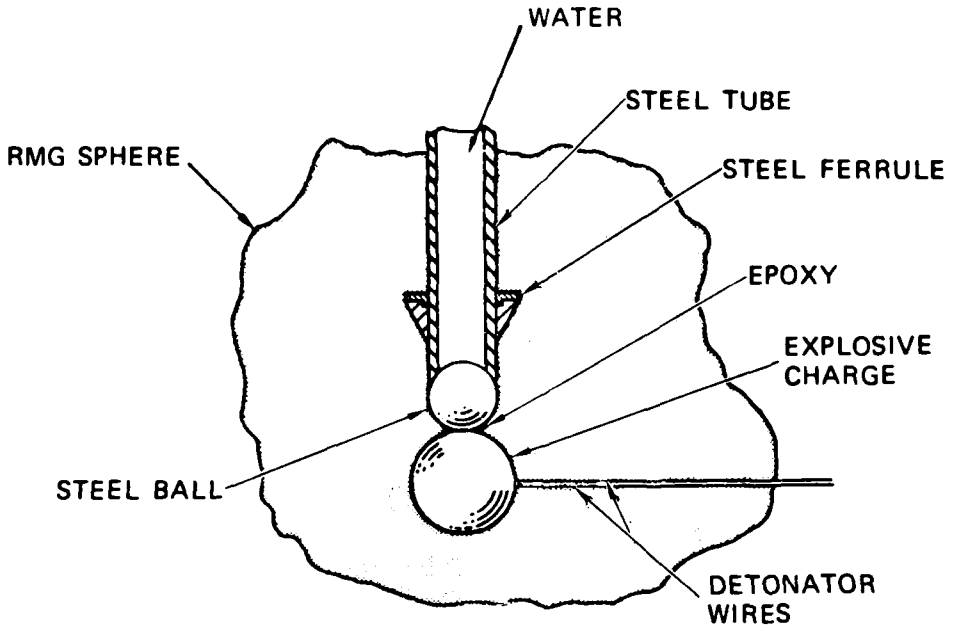

(a) INITIAL CONFIGURATION

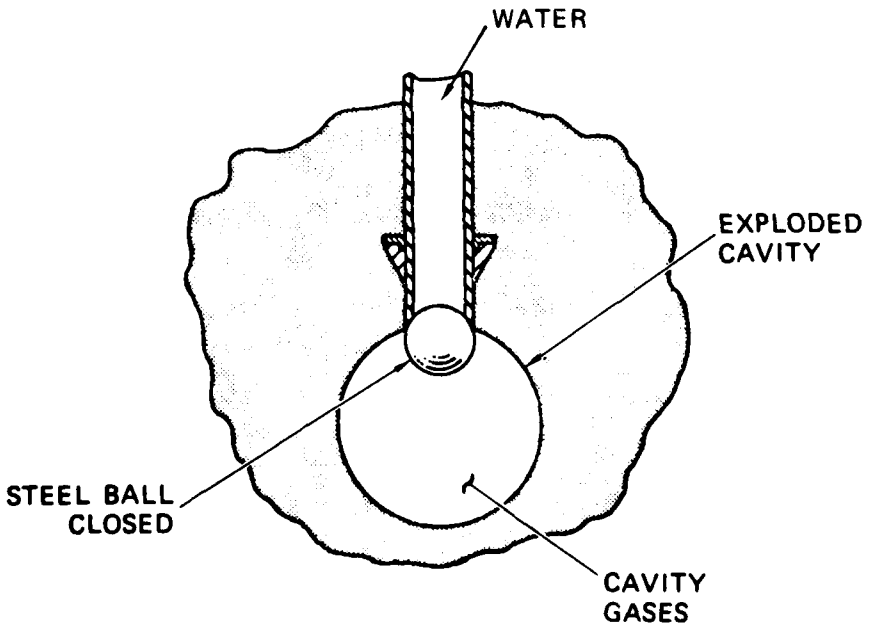

(b) CHARGE EXPLODED

MA-5958-96A

FIGURE 2.6 SEQUENCE OF OPERATIONS FOR UNVENTED EXPLODED CAVITY TESTS

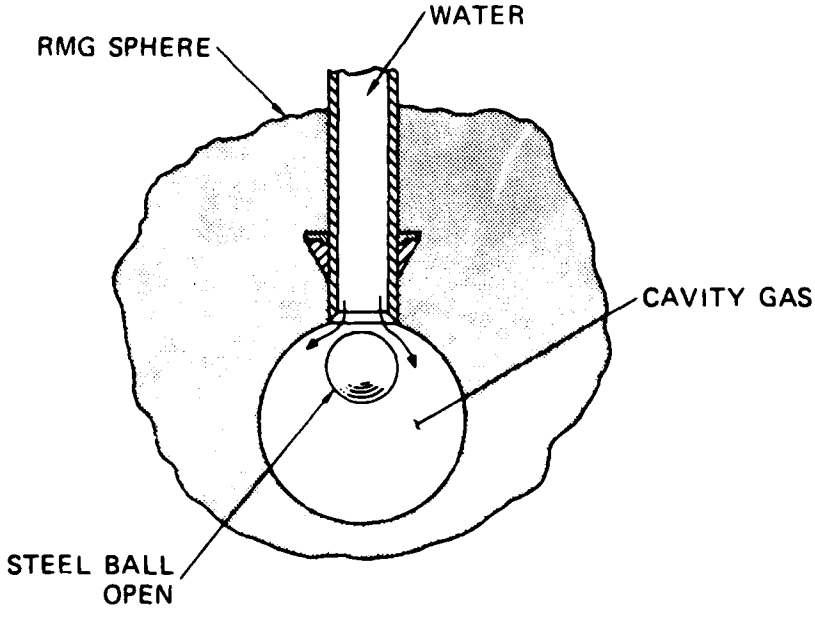

(c) START OF HYDROFRACTURE PROCESS

MA-5958-97A

FIGURE 2.6 SEQUENCE OF OPERATIONS FOR UNVENTED EXPLODED CAVITY TESTS (Concluded)

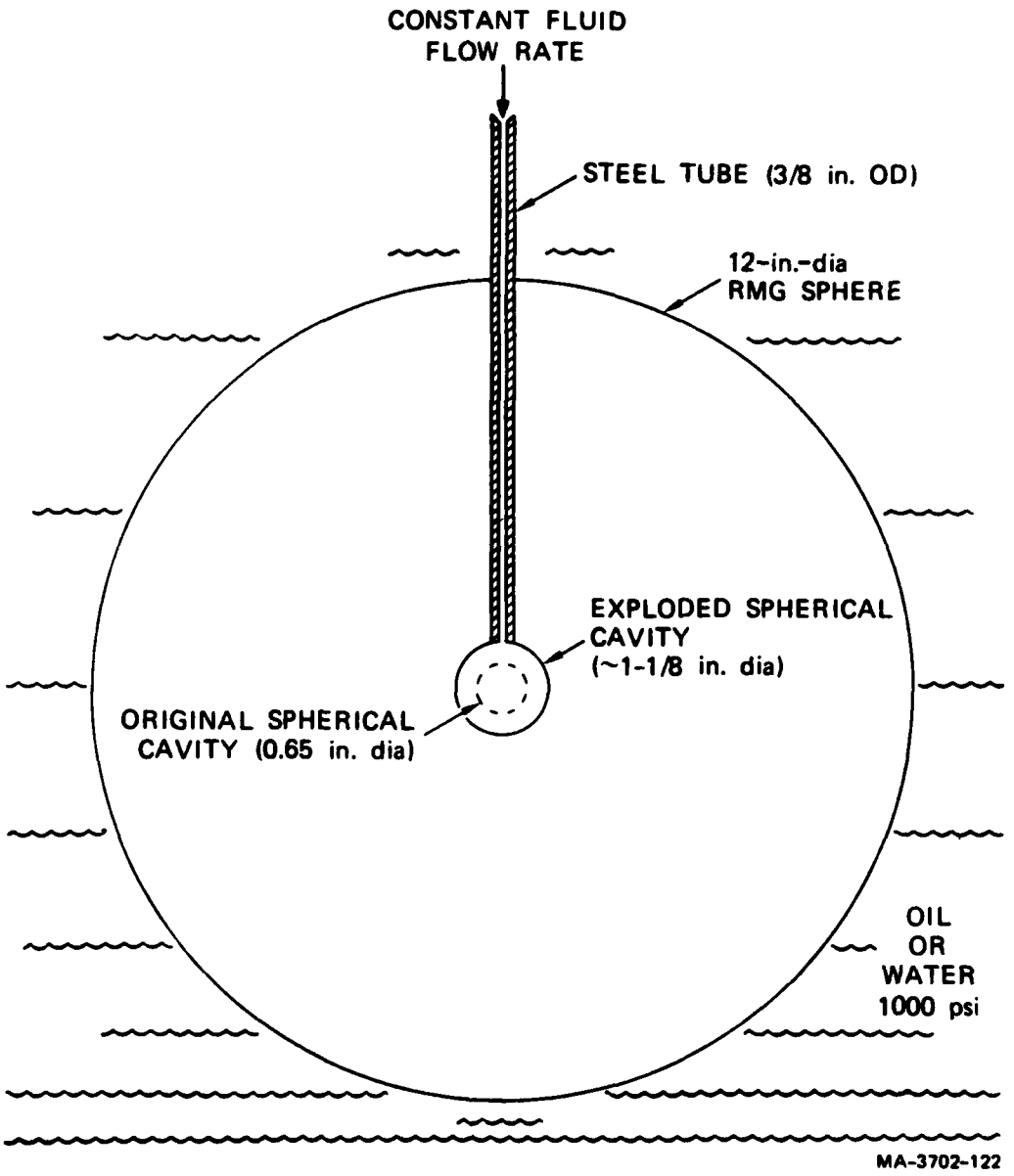

FIGURE 2.7 BASIC CONFIGURATION FOR VENTED EXPLODED CAVITY TESTS

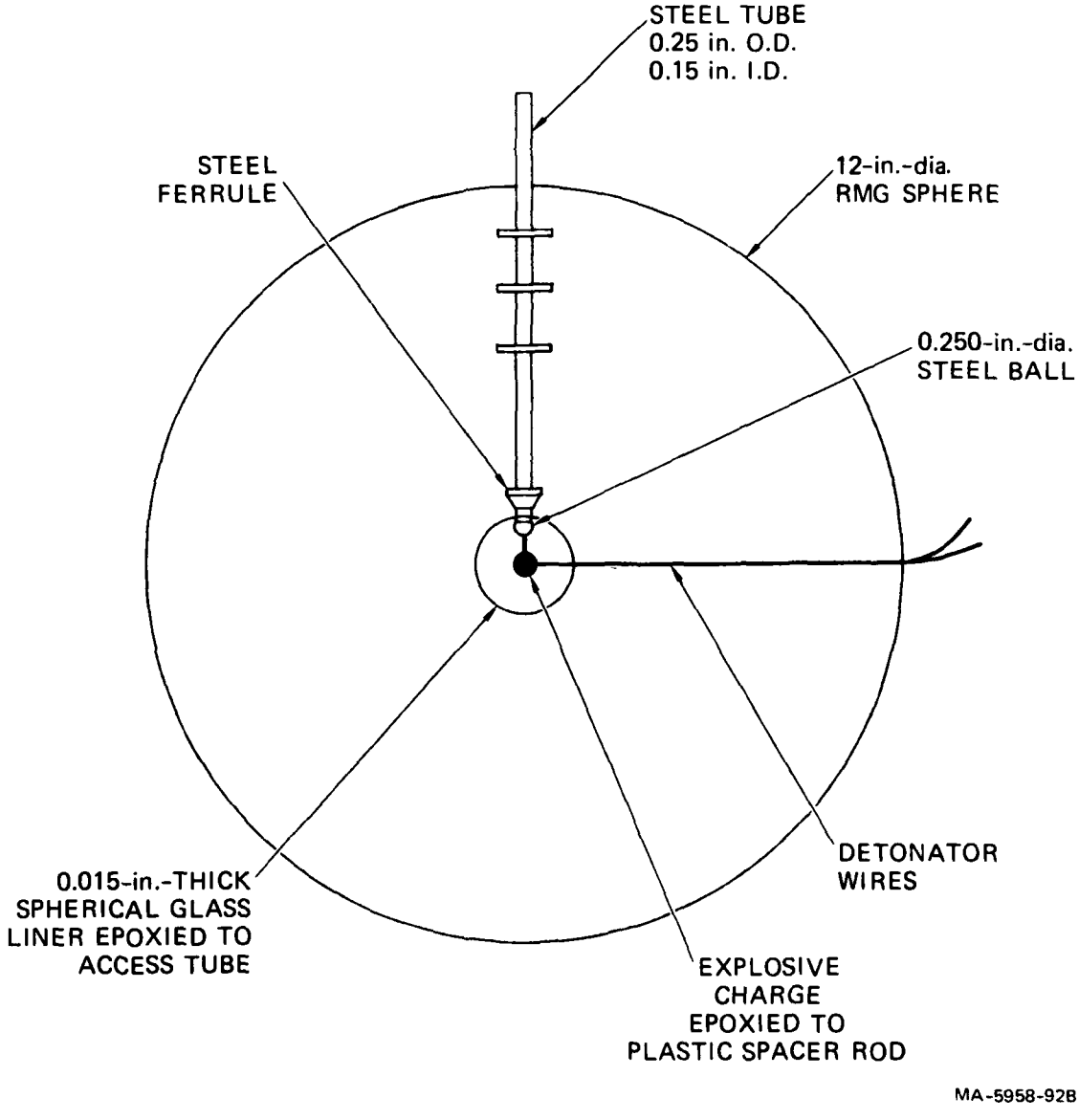

FIGURE 2.8 OVERALL CONFIGURATION FOR UNCOUPLED EXPLODED CAVITY TESTS

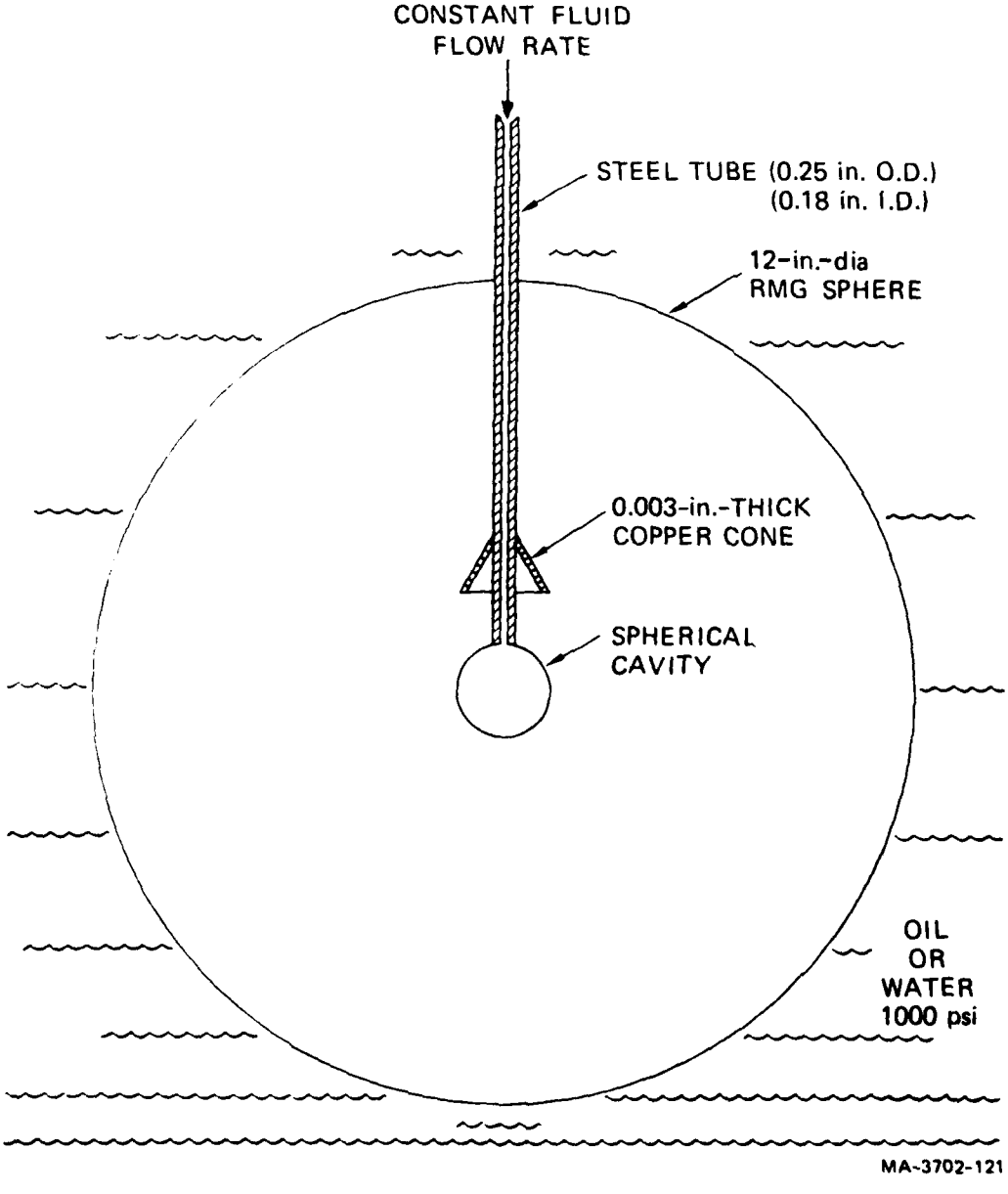

FIGURE 2.9 BASIC CONFIGURATION FOR UNEXPLODED CAVITY TESTS

2.3 INSTRUMENTATION

Surface fracture resulting from hydrofracture and states of stress and strain resulting from charge detonation and hydrofracture were monitored by the following sensors:

- Surface fracture gage (Figure 2.10)
- Embedded strain gage (Figure 2.11)
- Embedded ytterbium stress gage
- Embedded flat jack stress gage.

In addition, relevant particle velocity records that were generated during an independent laboratory study,[11] were incorporated into these results.

Surface Fracture Gage

Surface fracture of a grout sphere was detected by means of a 1/16-inch-wide (1.59-mm) stripe of electrically conductive silver-based paint. Two copper tabs were first embedded in the surface of the sphere during casting. After the grout was cured, the paint stripe was positioned to connect the tabs to cover a desired region. During hydrofracture the resistance from tab to tab was monitored. Visual inspection of the surface of the sphere during hydrofracture showed that a hairline crack in the grout is sufficient to break the paint and produce a noticeable resistance change in the gage. Typical surface regions covered by the gage are shown in Figure 2.10. Initial gage resistance, which is a function of length, was 100 to 200 ohms for the gage shown. Final resistance, which is a measure of electrical conductivity through the grout was 40,000 ohms.

Embedded Strain Gage

Radial and circumferential strain components in a grout sphere were measured by means of a standard Constantan foil strain gage rosette. The foil was first potted in a sphere of Castall 300 (RT-1 hardener) epoxy, which has elastic properties similar to that of grout. The entire unit was then cast in grout. Positioning was maintained by means of supporting threads and lead wires, as shown in Figure 2.11. The Castall protects the

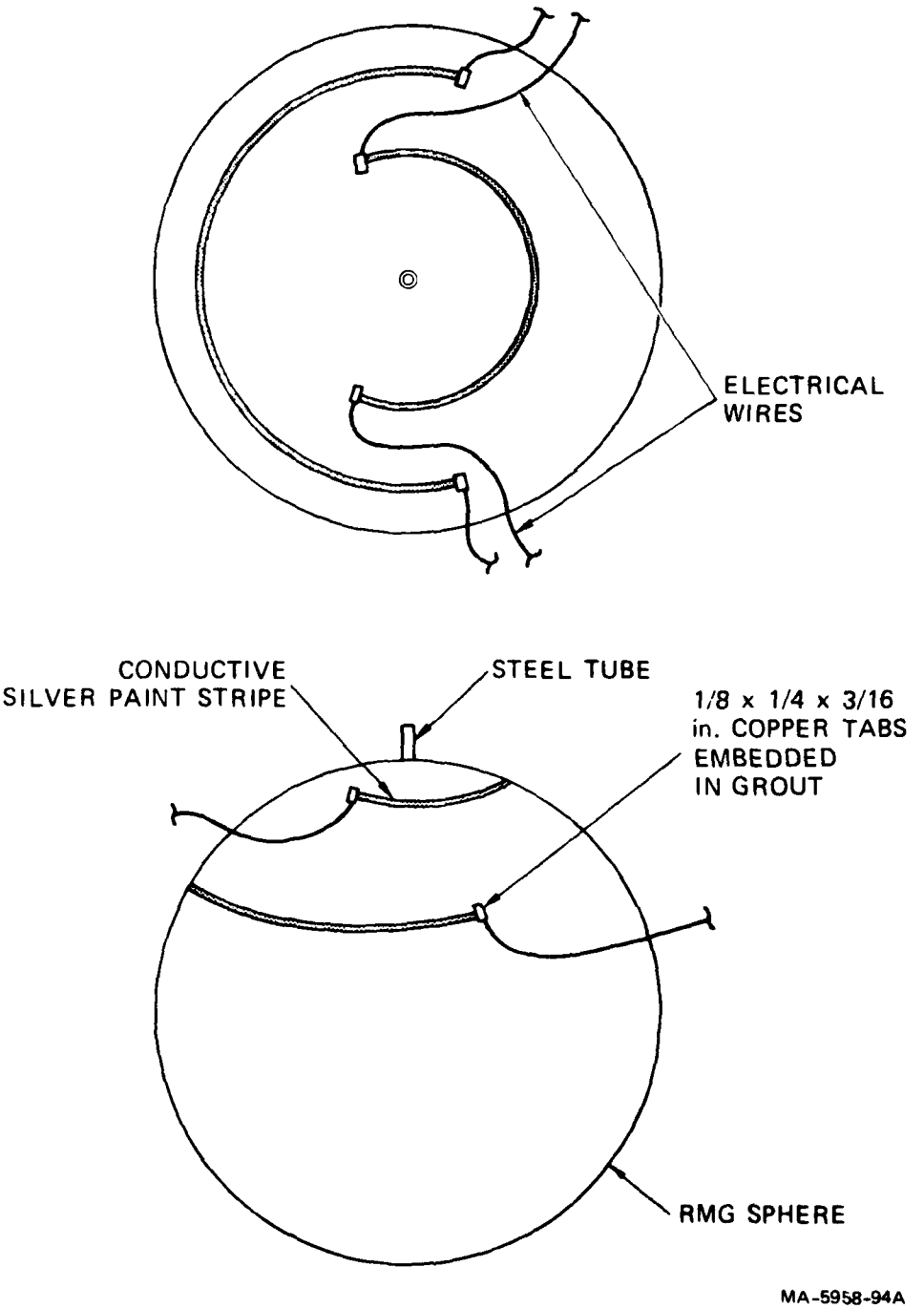

FIGURE 2.10 SURFACE FRACTURE GAGES

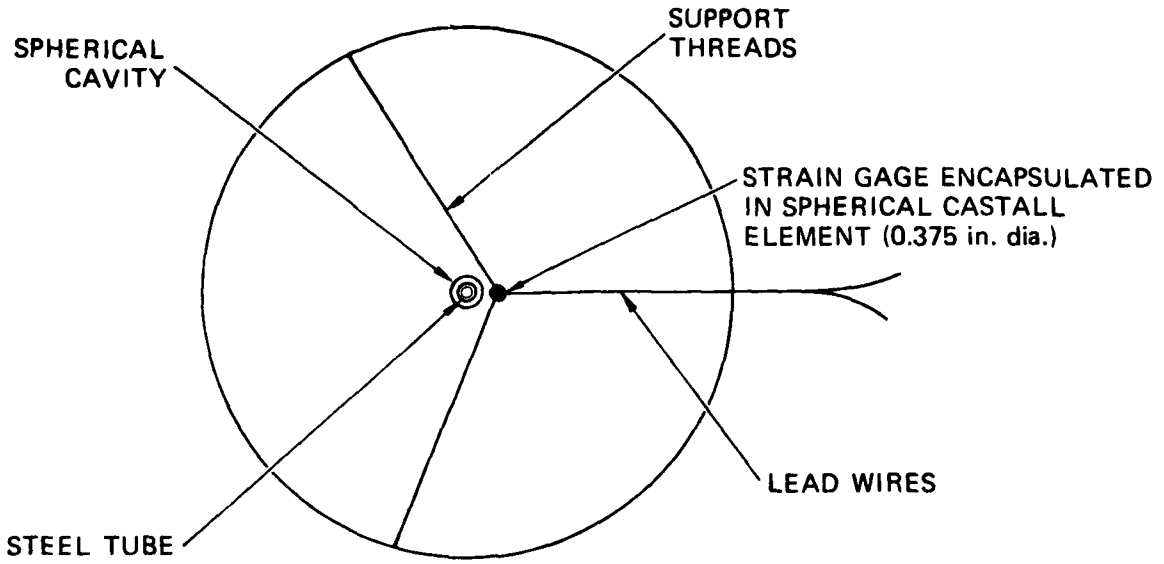

(a) TOP VIEW

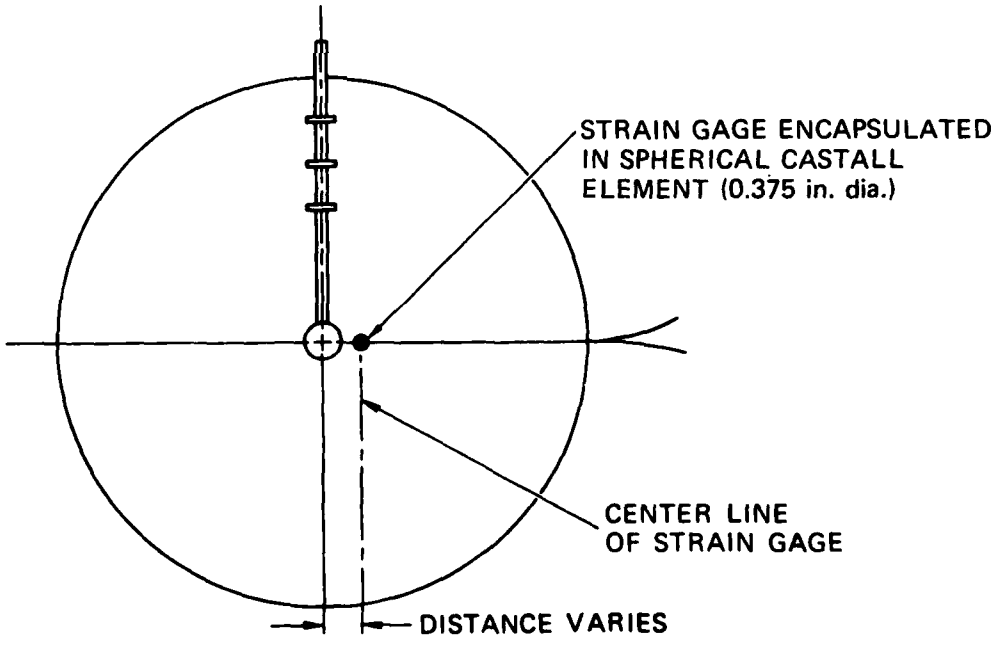

(b) SIDE VIEW

MA-5958-95A

FIGURE 2.11 EMBEDDED STRAIN GAGE

gage from sand particles and assures that the foil remains flat. An active gage length of 1/32 inch (0.79 mm) allows for reasonably accurate strain measurements even at a distance of two cavity radii from the center of the sphere where strain gradients are steep. Static calibration tests performed on axially and hydrostatically loaded grout cylinders showed that strains from an embedded gage were in good agreement with strains predicted by elasticity theory.

Embedded Ytterbium Stress Gage

A stress gage containing a ytterbium element for measuring dynamic and residual stress was brought to an advanced stage of development.

Initially, ytterbium and carbon were selected as candidate materials for the piezoresistive stress gage because of their sensitivity to the expected levels of residual stress. Each element was cycled under hydrostatic compression to 70,000 psi (482.63 MPa). The ytterbium element exhibited no hysteresis with each loading cycle and was judged a suitable gage material. The carbon element, however, showed considerable hysteresis and was eliminated from future consideration.

The ideal gage configuration would have the sensing element in a fluid environment, with the fluid pressure dependent on a single component of the applied stress. However, the small displacements associated with stress relaxation and the thermal effects associated with fluid compression make such a package impractical for use in the containment experiments. A practical gage configuration is a sensing element sandwiched between stiff steel diaphragms welded together along two opposite edges. The overall modulus of the package in uniaxial compression should equal that of the RMG.

A stress gage package was designed and assembled containing a ytterbium element for measuring stress and a constantan element for measuring temperature because the gage calibration depends on the temperature. The overall modulus of the package in uniaxial compression was made equal to that of the RMG by using a suitable thickness of heat-sealing Mylar for electrical insulation. The gage was designed to be sensitive to the component of stress normal to the diaphragms and insensitive to all other stress components.

Figure 2.12 shows the results of calibration tests in oil and in RMG. In oil, the gage was cycled to 16,500 psi (113.76 MPa). The corresponding resistance change of the ytterbium element in the package followed the path associated with the hydrostatic coefficient of ytterbium. Hence, the gage showed sensitivity to all components of applied stress and not just the component normal to the faces of the package.

In an RMG cylinder, the gage was first cycled to 2000 psi (13.79 MPa) hydrostatic pressure. For sufficiently large applied pressure, the response of the ytterbium was again indicative of the hydrostatic coefficient. The deviation from the hydrostatic response for small applied pressure may have been caused by a bridging effect associated with imperfect contact between the gage and surrounding grout. This effect would have negligible influence on measurements of residual stress decay made near an exploded cavity.

The gage was further tested in RMG by subjecting the cylinder to uniaxial compression. The cylinder was first cycled to 2610 psi (18.00 MPa), and the ytterbium again showed a hydrostatic response with an offset for small applied loads. Finally, the cylinder was tested to 3480 psi (23.99 MPa) and the load was held constant. Under this load, the response of the ytterbium tended toward the hydrostatic coefficient line and the RMG specimen eventually fractured. Hence the material matrix of the RMG appears to have deteriorated with time under constant load, resulting in a more nearly hydrostatic stress state in the vicinity of the gage.

The results suggest a modified design incorporating welding around all edges of the steel diaphragms (apart from the lead exit). The fully welded design has been reliable in larger scale versions.

Embedded Flat Jack Stress Gage

A flat jack package was designed for measuring residual stress in exploded cavity spheres. The gage consists of two edge-welded circular plates, a displacement gage sensitive to a plate motion of 0.004 mil (0.0001 mm), and an inlet tube for applying internal gas pressure to the package. The stress component normal to the surface of the 0.625-inch-diameter (1.59-cm) plates is monitored. The gage was calibrated hydrostatically in water and uniaxially in a grout cylinder.

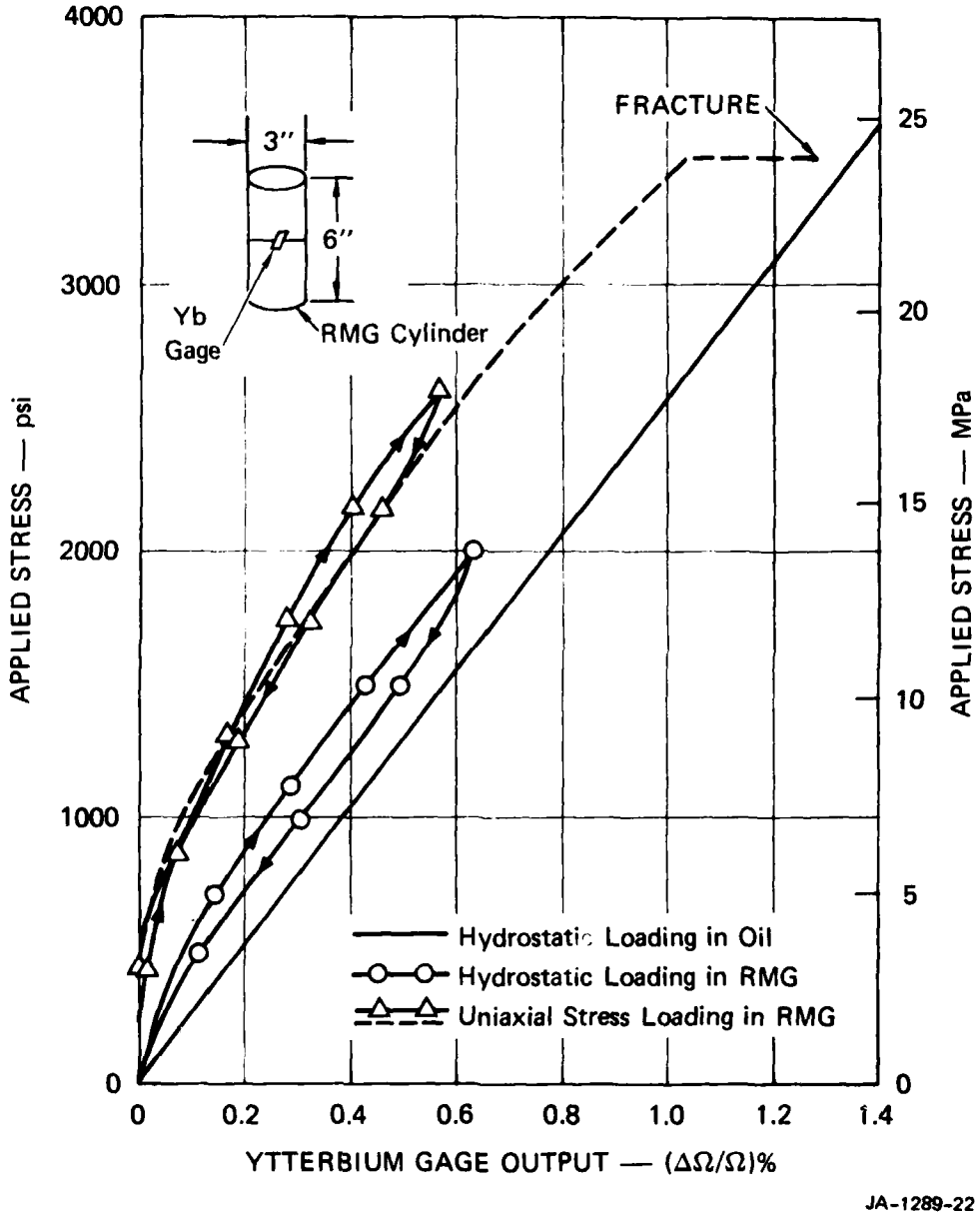

FIGURE 2.12 RESPONSE OF YTTERBIUM STRESS GAGE IN OIL AND IN RMG 2C4

In water, the gage accurately monitored hydrostatic pressure as high as 2000 psi (13.79 MPa). Calibration was not attempted at higher pressures. In a grout cylinder loaded in uniaxial compression to 1000 psi (6.90 MPa), the gage responded to the external load such that the internal pressure required to balance a given applied stress was approximately half the value of the applied stress. This response indicates a bridging of the gage by the surrounding grout. However, the calibration was reproducible under repeated cyclic loading.

Embedded Particle Velocity Gage

Particle velocity records associated with charge detonation in rock-matching grout are shown in Figure 2.13. The results, which were taken from a recent laboratory study of stress waves crossing fault planes,[11] provide additional data for verifying the calculations. Radial velocity 4 cm from the center of the charge was measured. An average profile based on the four records in Figure 2.13 yields a time of arrival of 12 μs, a peak particle velocity of 7.0 m/s, and a reversal of motion at 41 μs. Figure 2.14 shows the decay of maximum particle velocity as the distance (r) from the charge is increased. For $r > 4$ cm the decay is of the form A/r^n, where A is a constant and $n = 1.4$. This result is consistent with elasticity theory which requires that $1 \leq n \leq 2$ for an elastic spherical wave.

2.4 CHARGE REPRODUCIBILITY

Reproducibility of the explosive source is a basic requirement of exploded cavity tests and has been demonstrated in the past.[6,7] To periodically monitor charge reproducibility, we used a quartz gage to measure the reflected pressure pulse generated in the overburden fluid during exploded cavity tests. Measurements were made at the bottom of the pressure vessel directly below the charge as shown in Figure 2.2. Although the nominal distance from charge center to gage was 6-5/8 inches (17.0 cm), a tolerance of 1/8 inch (0.318 cm) should be allowed.

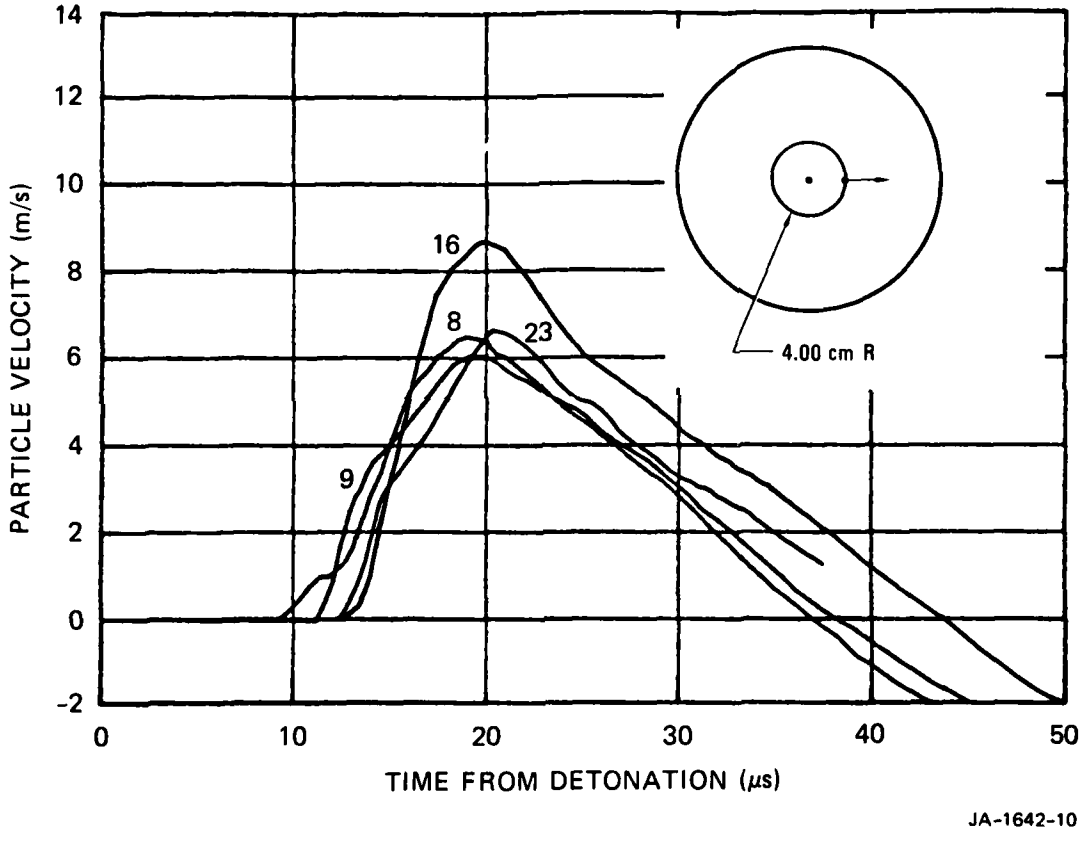

FIGURE 2.13 PARTICLE VELOCITY PLOTS FROM SYMMETRY TESTS 8, 9, 16, AND 23

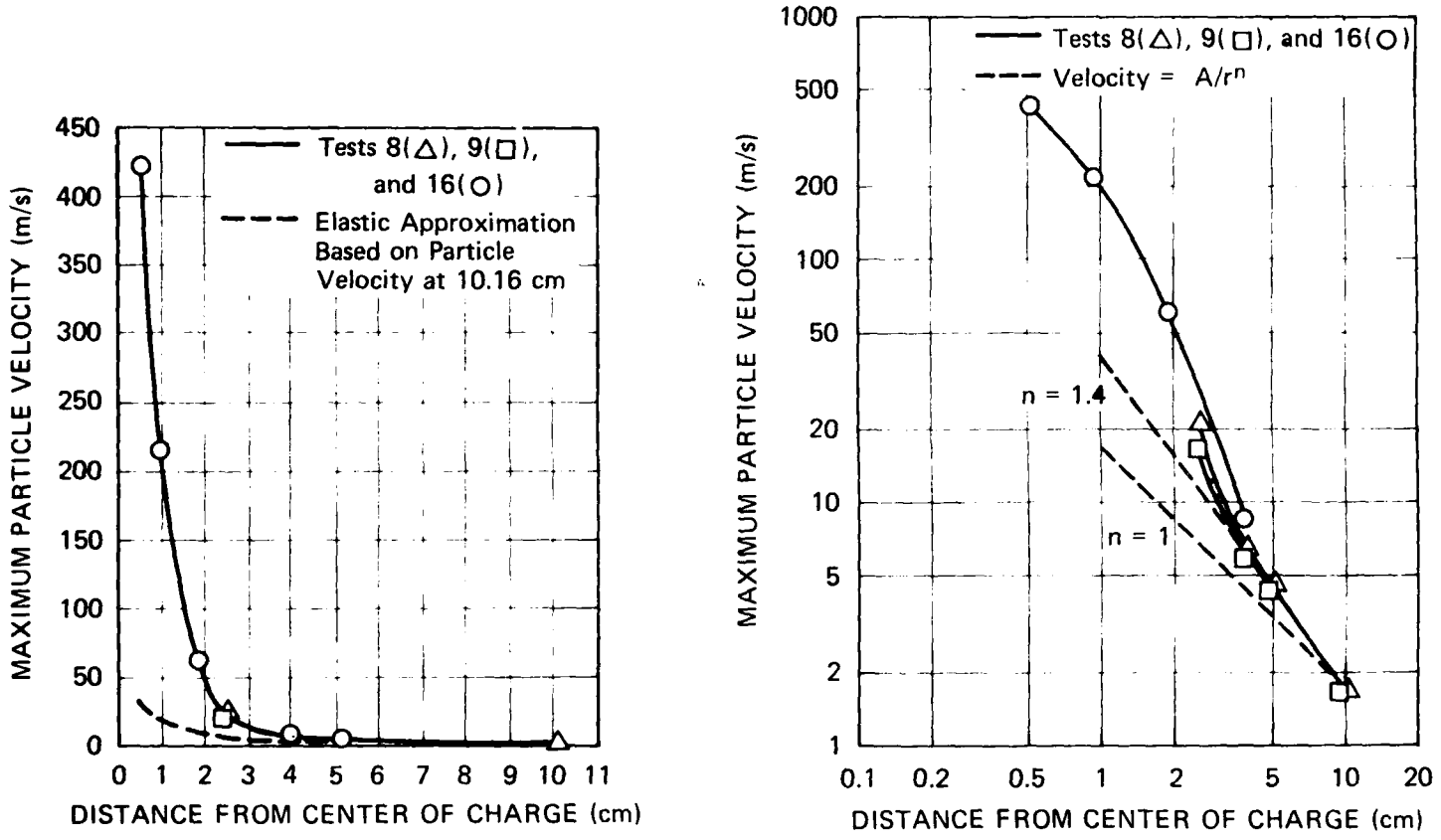

(a) MAXIMUM PARTICLE VELOCITY PROFILE

(b) LOGARITHMIC PLOT OF MAXIMUM PARTICLE VELOCITY PROFILE

JA-1289-15

FIGURE 2.14 MAXIMUM PARTICLE VELOCITY PROFILES FROM SYMMETRY TESTS 8, 9, AND 16

A summary of the charge reproducibility results is given in Table 2.1, where tests are categorized according to the coupling parameter. Maximum reflected pressure and total reflected impulse are listed for each test.

Reflected pressure pulses from fully coupled tests are shown in Figure 2.15. The corresponding impulse curves are shown in Figure 2.15. The average maximum reflected pressure for these tests is 784 psi (5.41 MPa), with a maximum deviation of 15.5%. The corresponding average total reflected impulse and maximum deviation are 9.6 psi•ms (0.066 MPa•ms) and 9.0%. For calculation of total impulse, the pressure pulse was assumed to end when the pressure dropped to the initial value as shown in Figure 2.15.

Reflected pressure pulses from uncoupled cavity tests are shown in Figures 2.16 and 2.17. The corresponding impulse curves are shown in Figures 2.16 and 2.17. For comparison, typical pulses from fully coupled tests are also shown. The maximum pressure and total impulse are similar for all tests, indicating that the uncoupled cavities were filled with a relatively uncompressible medium before charge detonation. The subsequent hydrofracture records (described in Section 3) indicate water-filled cavities. The pressure profiles show a second peak that becomes more pronounced as the uncoupling is increased. This feature is attributed to reflections within the exploded cavity.

In conclusion, the results show pulse shapes that are strikingly similar for a given coupling parameter, indicating a reproducible release of energy from the charge in all cases.

Table 2.1

SUMMARY OF CHARGE REPRODUCIBILITY RESULTS

Test No.	Nominal Coupling Parameter (initial cavity radius/ charge radius)	Maximum Reflected Overpressure (psi)[a]	Total Reflected Impulse (psi•ms)[a]
248	1	904	10.09
249	1	901	9.54
250	1	662	8.74
251	1	704	9.48
254	1	748	10.18
255	1.5	801	8.52
256	1.5	803	8.62
252	3	896	10.59
253	3	714	9.63

[a] 1 psi = 6.895 kPa.

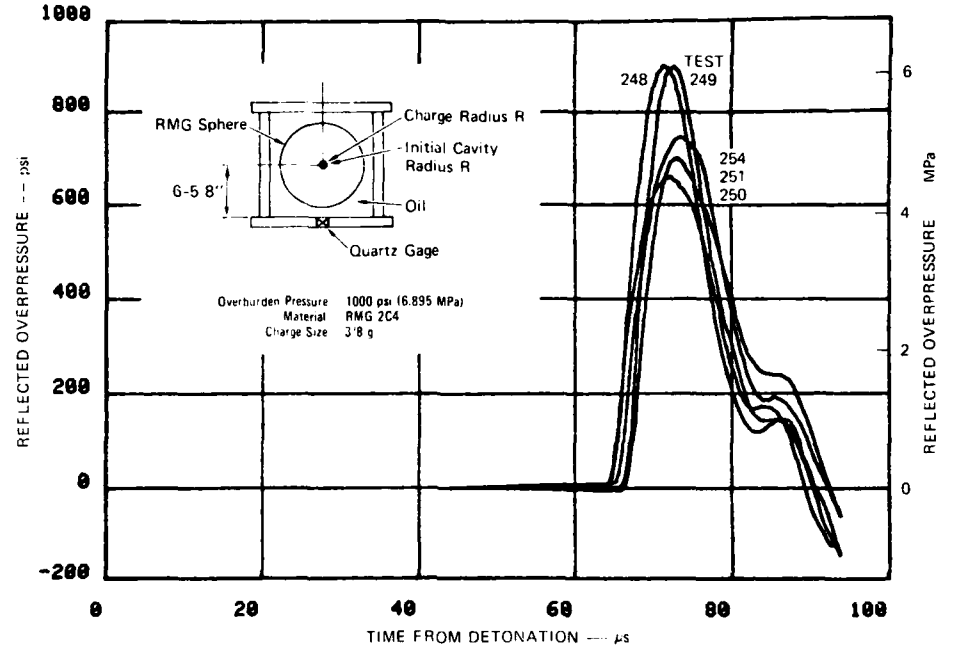

(a) REFLECTED PRESSURE PULSES

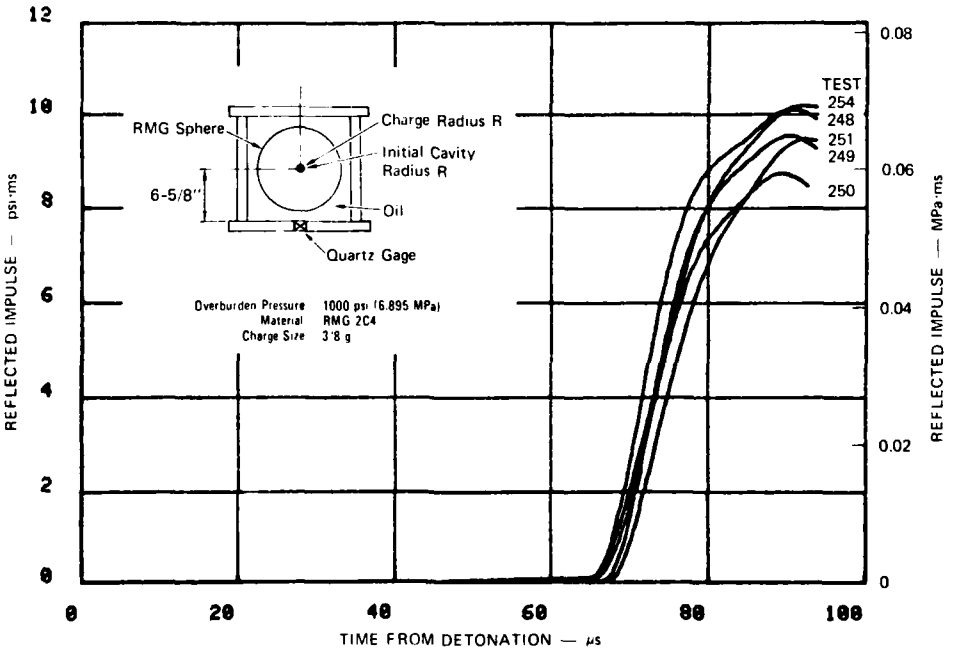

(b) REFLECTED IMPULSE

JA 1289 16

FIGURE 2.15 REFLECTED PRESSURE PULSES AND IMPULSE FROM COUPLED EXPLODED CAVITY TESTS 248, 249, 250, 251, AND 254

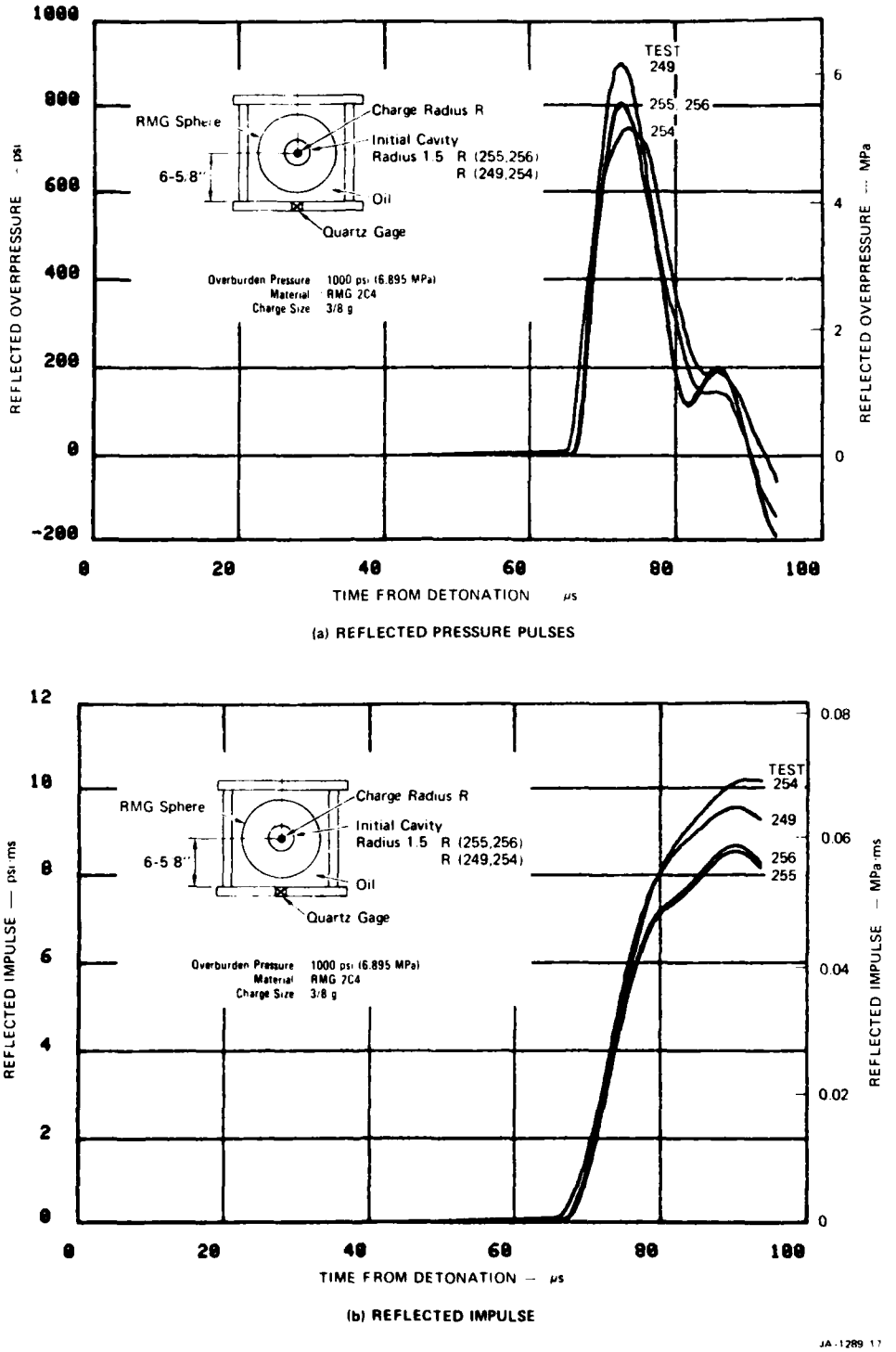

FIGURE 2.16 REFLECTED PRESSURE PULSES AND IMPULSE FROM COUPLED EXPLODED CAVITY TESTS 249 AND 254 AND UNCOUPLED EXPLODED CAVITY TESTS 255 AND 256

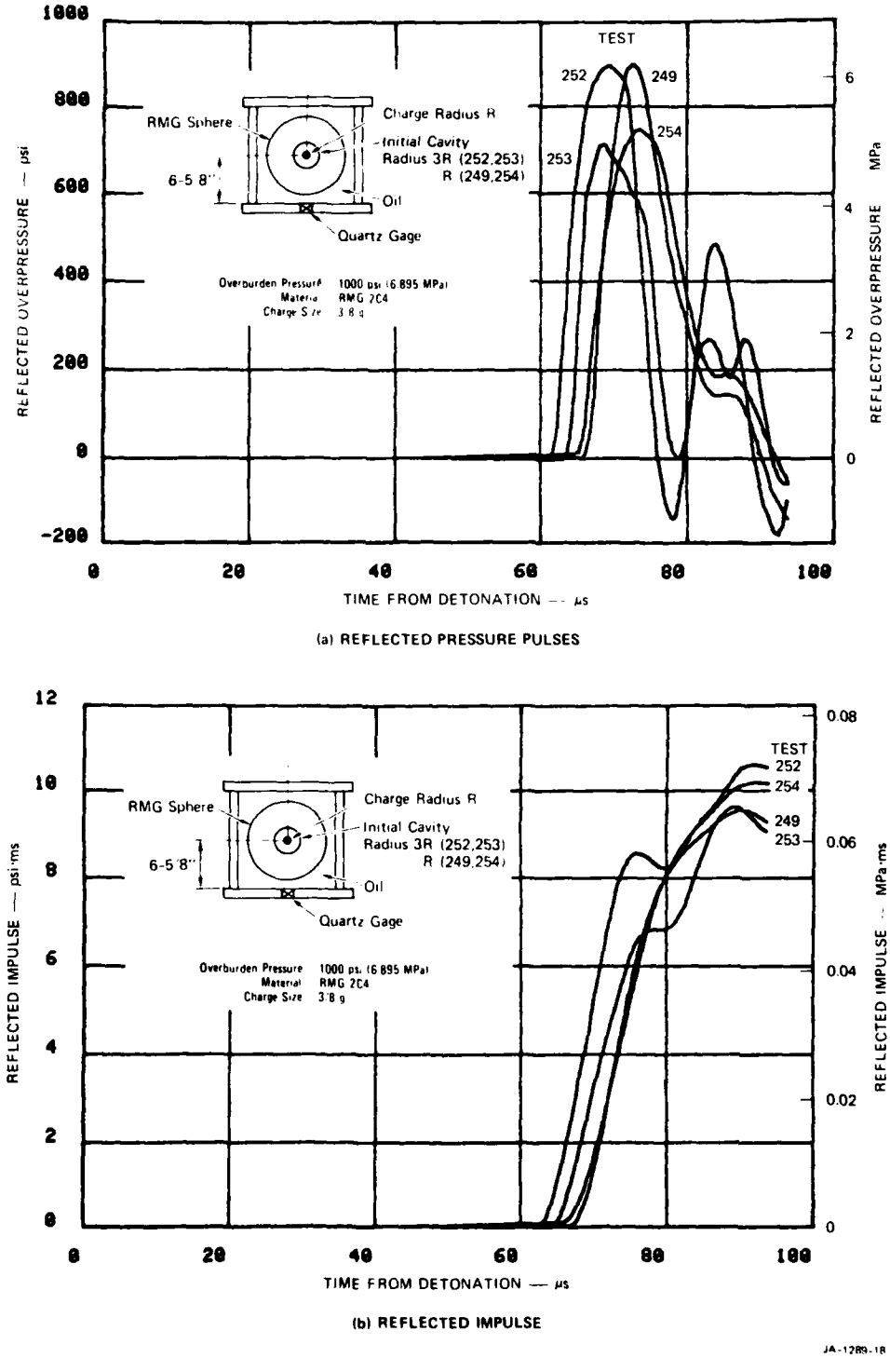

FIGURE 2.17 REFLECTED PRESSURE PULSES AND IMPULSE FROM COUPLED EXPLODED CAVITY TESTS 249 AND 254 AND UNCOUPLED EXPLODED CAVITY TESTS 252 AND 253

SECTION 3

HYDROFRACTURE RESULTS

3.1 TEST SERIES

Tests were performed on unexploded and exploded cavity spheres so that by a comparison of hydrofracture records we could assess the contribution of residual stress to containment. The experiments were specifically designed to provide the influence on containment of various factors such as flow rate, stress relaxation, charge uncoupling, and unloading due to cavity gas pressure decay. In addition, sensors were embedded to provide a direct measure of the stress and strain associated with charge detonation and hydrofracture. This section provides a complete description of the results. Conclusions based on these findings are contained in the summary of Section 1.2.

The types of experiments and the principal observations are summarized in Table 3.1. Unexploded cavity tests are grouped in series 1 and 2; exploded cavity tests are grouped in series 3 through 8. In general, at least two tests were performed in each series to establish a measure of reproducibility. The specific areas of investigation were as follows:

- Flow rate (series 1 and 3). The rate of fluid flow is a parameter that establishes the time required to hydrofracture. In unexploded cavity tests, this parameter allows us to vary the duration of creep and fluid motion due to porous flow. In exploded cavity tests, this parameter allows us to vary the duration of residual stress relaxation and decay of cavity gas pressure. Flow rates ranged from 4.26 to 122.4 cm^3/min, with the highest value chosen so that hydrofractures could be performed within the scaled time of relevance (5 seconds) for an underground nuclear test (using a scale factor of 1200 gives 1 hour, 40 minutes).

- Strain measurements (series 2 and 7). Charge detonation results in a region of residual stress and corresponding plastic strain surrounding an exploded cavity. The strain approaches an elastic state at distances greater than 6 cavity radii (5.7 cm) from the center of detonation. Strain

Table 3.1

SUMMARY OF CONTAINMENT INVESTIGATIONS

Series	Purpose or Parameter	Test Results (Figure)	Initial Cavity Diameter (in.)	Flow Rate (cm^3/min)	Test Numbers	Observations
Unexploded Cavity Experiments						
1	Flow Rate	3.1	0.750	4.26	93, 94 160,161	Similar hydrofracture records for flow rates of 4.26 and 40.8 cm^3/min.
				40.8	225,226 230	
2	Strain Measurements	3.3	0.750	40.8	225	Hydrofracture strain nearly twice the value predicted by elasticity theory.
Exploded Cavity Experiments						
3	Flow Rate	3.4 3.8 3.9	0.404	4.26	158,159 169,170	Fracture initiation pressure increases 97% as flow rate is increased from 4.26 to 40.8 cm^3/min. No further increase for a flow rate of 122.4 cm^3/min.
				40.8	227,229 232,249	
				122.4	244,245 248,254	
4	Stress Relaxation	3.10	0.404	40.8	234,250 251	Stress relaxation for 10 sec reduces fracture initiation pressure by 29%.
5	Uncoupled Cavity	3.11	0.594	122.4	255,256	Water-filled cavities with coupling parameters of 1.5 and 3 resulted in 29% and 59% reductions in fracture initiation pressure.
			1.219		252,253	
6	Vented Cavity	3.12 3.14	0.404	4.26	162,163 164,177	Similar fracture initiation pressures for flow rates of 4.26 and 61.2 cm^3/min. Gas-fracture record similar to hydrofracture record of unexploded cavity.
				61.2	242,243	
				GAS	246	
7	Strain Measurement	3.15 3.16	0.404	40.8	250,251	Residual strain decay of 30% to 50% observed near an exploded cavity during the first 9 seconds following charge detonation.
				None	243	
8	Stress Measurements	None	0.404	None	242,243 246,247	Further development of ytterbium and flat jack stress gage packages required.

decay probably implies residual stress relaxation. A strain gage rosette monitored the decay of radial and circumferential strain components in a region of small plastic deformation. The static radial strain component associated with hydrofracture of unexploded cavity spheres was also measured.

- Stress relaxation (series 4). The explosively formed residual stress field surrounding an exploded cavity is degraded with time due to material relaxation. Hydrofracture experiments, in which the cavity pressure was held constant for 10 seconds following charge detonation, were performed on unvented exploded cavity spheres to isolate and study stress relaxation in rock-matching grout.

- Uncoupled cavity (series 5). In a fully coupled exploded cavity test, the explosive source is in direct contact with the surrounding medium. In an uncoupled exploded cavity test, an annular region of highly compressible material separates the explosive source from the surrounding medium. The coupling parameter (ratio of initial cavity diameter to charge diameter) determines the degree of uncoupling. Hydrofracture tests were performed on unvented exploded cavity spheres with coupling parameters of 1.5 and 3.

- Vented cavity (series 6). Release of the detonation products from an exploded cavity before hydrofracture provides the limiting case of complete unloading for the unvented hydrofracture tests. Cavity venting also enhances relaxation of the dynamically produced residual stress field surrounding an exploded cavity. Hydrofracture tests were performed on vented exploded cavities at a flow rate of 61.2 cm^3/min. A gasfracture test was also performed.

- Stress measurements (series 8). Embedded stress gages (ytterbium and flat jack) were used in an attempt to monitor the radial component of dynamic stress and decaying residual stress near an exploded cavity. These measurements were intended to establish directly the existence of residual stresses and relaxation of rock-matching grout.

3.2 UNEXPLODED CAVITY TESTS

Series 1 - Flow Rate

Hydrofracture tests were performed on unexploded cavity rock-matching grout (RMG 2C4) spheres to provide comparison data for a parameter study of flow rate. The configuration shown in Figure 2.9 was used in these

tests. A cavity diameter of 3/4 inch (1.90 cm) was chosen because it corresponds to the exploded cavity diameter generated by a 3/8-gram charge in previous tests. The external pressure applied to each sphere was fixed at 1000 psi (6.895 MPa) to simulate the hydrostatic overburden pressure in nuclear tests typically conducted at a depth of 1100 feet (335 m) in tuff with a density of 2.1 g/cm^3. Dyed water was the hydrofracture fluid.

Hydrofracture records from tests 225, 226, and 230, in which the flow rate was 40.8 cm^3/min, are shown in Figure 3.1. For comparison, hydrofracture records from previously reported[7] tests 93, 94, 160, and 161, in which the flow rate was 4.26 cm^3/min, are also shown. The similarity of the pressure records indicates that flow rate has a relatively minor effect on hydrofracture for the range tested. The results are representative of unexploded cavity tests in that a smooth increase in pressure is followed by a sharp drop to form a well-defined peak. Previous fracture initiation studies[7] have shown that the pronounced spike represents the initiation of a crack in the wall of the cavity. Fracture initiation pressures for tests 225, 226, and 230 were 1900, 1880, and 1770 psi (13.10, 12.96, and 12.20 MPa), respectively, an average of 1850 psi (12.75 MPa). For tests 93, 94, 160, and 161, the respective fracture initiation pressures were 1950, 1940, 1820, and 1770 psi (13.44, 13.38, 12.55, and 12.20 MPa), an average of 1870 psi (12.89 MPa).

After fracture initiation, a crack continues to grow as cavity pressure decays slowly to a plateau. This steady-state pressure provides a measure of flow resistance along the fracture plane. For the higher and lower flow rates, the average steady-state pressure was 1180 psi (8.136 MPa) and 1330 psi (9.170 MPa), respectively. Hence, the higher flow rate produced a generally wider crack that offered less resistance to flow. As shown in Figure 3.1, a crack (C) was detected at the surface of the sphere in test 230 after 4.6 cm^3 of flow. This volume is measured from the point of fracture initiation.

Because the pressure-volume curves in Figure 3.1 were plotted on the basis of a constant rate of fluid flow, we can obtain pressure-time

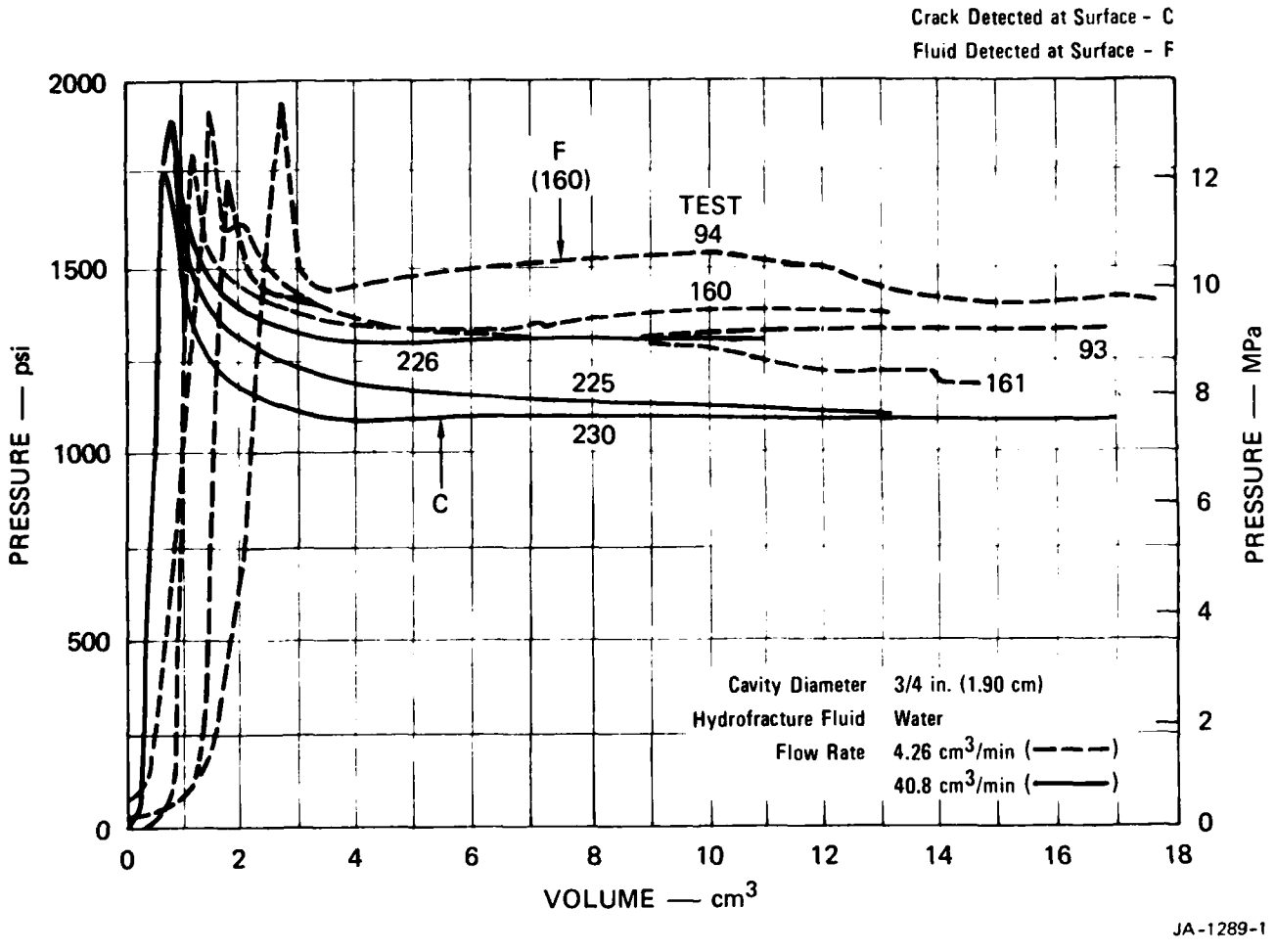

FIGURE 3.1 HYDROFRACTURE PRESSURE FOR UNEXPLODED CAVITY TESTS 93, 94, 160, 161, 225, 226, AND 230 – FLOW RATE EFFECT

curves by applying the appropriate flow rate. Hence the average time to initiate a fracture in the higher and lower flow rate was 1.1 and 27.2 seconds, respectively.

Figure 3.2 shows a typical fracture surface associated with an unexploded cavity test. The uniformity of the dyed region suggests that the fracture initially propagated symmetrically from the cavity. Sectioning of the unexploded cavity spheres showed that a single planar fracture surface was produced by hydrofracture in each test. The fracture plane was randomly oriented.

Series 2 - Strain Measurements

The radial component of strain in an unexploded cavity sphere was measured by means of the strain gage package described in Section 2.3. Two packages were cast symmetrically about the cavity, in the plane of the equator, two cavity radii from the center of the sphere, as shown in Figure 3.3. Strains were generated by overburden and hydrofracture pressures.

Strain records from test 225, performed with a flow rate of 40.8 cm^3/min, are shown in Figure 3.3. Since the maximum experimental strains are elastic (less than 1000 μstrain), elasticity theory predictions based on the pressure record shown in Figure 3.1 are included. Separate theoretical predictions are shown for the Castall package and for RMG 2C4 because the elastic properties of these materials are similar but not identical. Calibration tests on a RMG cylinder containing a strain gage package and subjected to uniaxial and hydrostatic compression showed that the strains were consistent with the theoretical predictions for Castall. Hence, experimental hydrofracture results are compared to the theoretical predictions based on the material properties of Castall.

Although the experimental and theoretical strain records have the same general shape, experimental values are higher. An overburden pressure of 1000 psi (6.895 MPa) produced strains of 145 and 158 μstrain in the gages. The theoretical value is 140 μstrain. A fracture initiation pressure of 1900 psi (13.10 MPa) produced strains of 392 and 434 μstrain

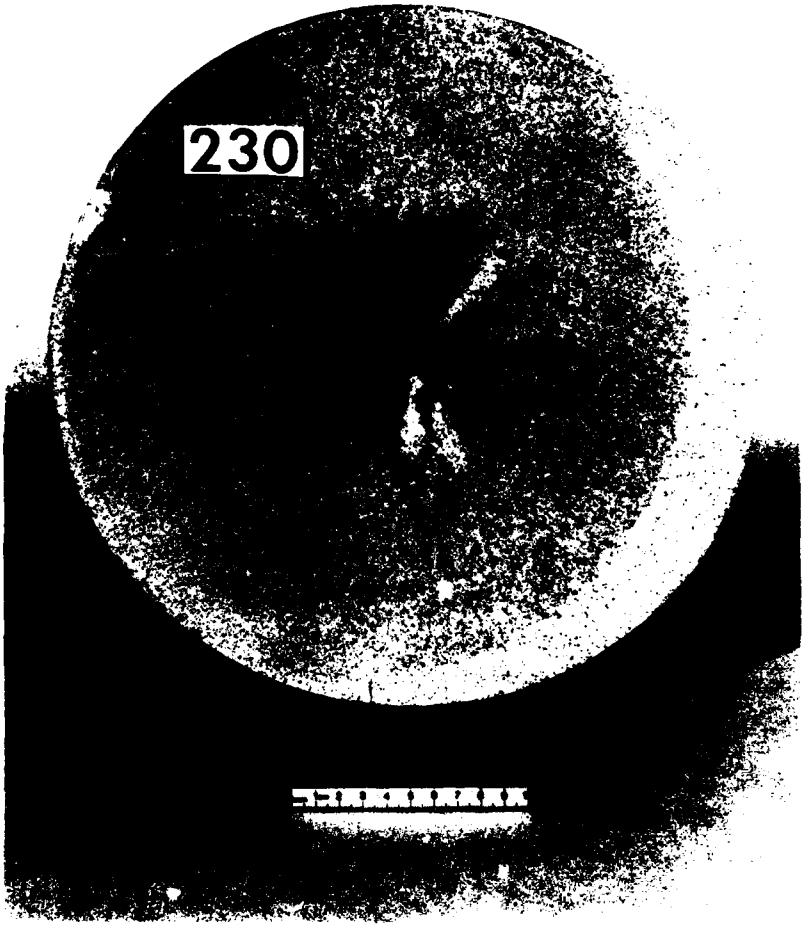

JP-1289-2

FIGURE 3.2 HYDROFRACTURE FROM UNEXPLODED CAVITY
TEST 230 — FLOW RATE EFFECT

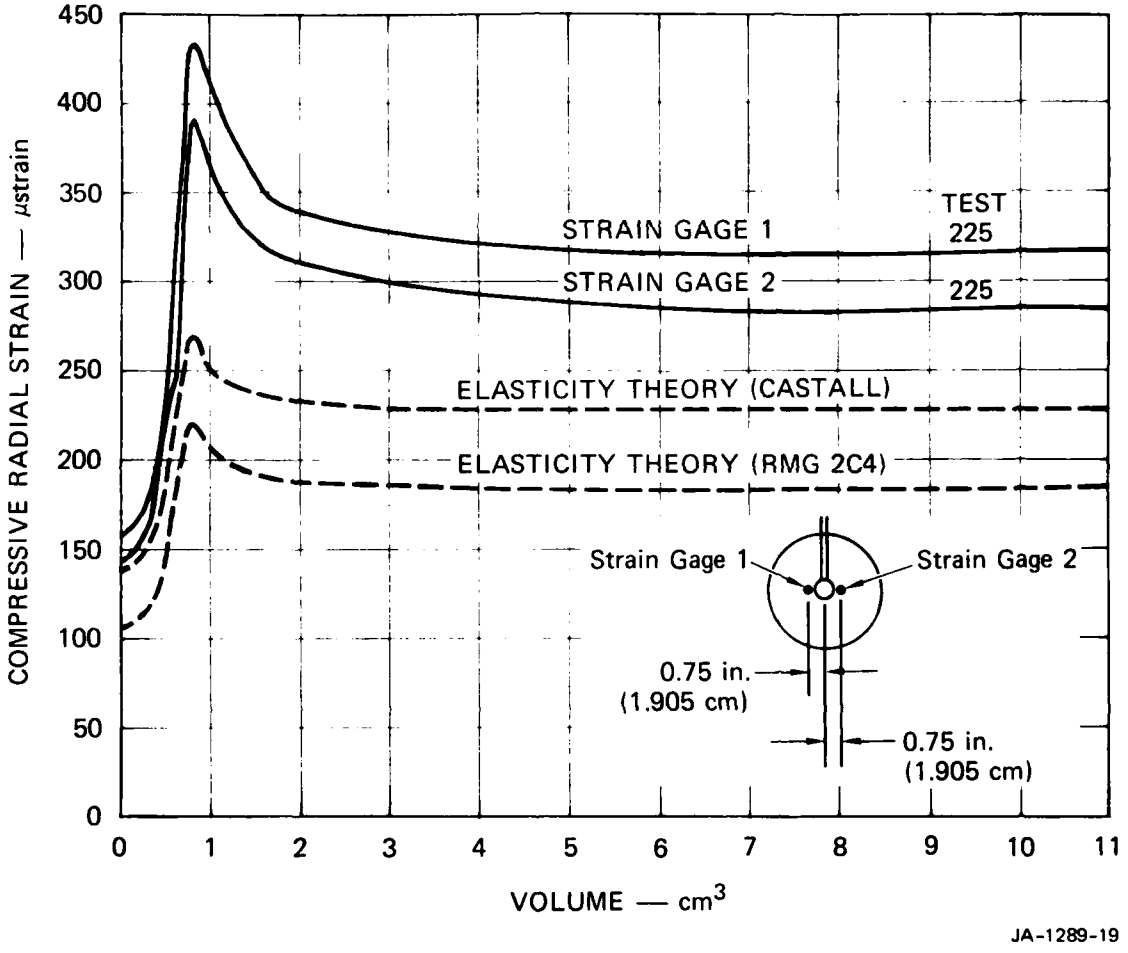

FIGURE 3.3 HYDROFRACTURE STRAIN FOR UNEXPLODED CAVITY TEST 225

in the gages. The theoretical value is 270 μstrain. The subsequent fracture plane intersected both gages. The theory neglects fracture propagation and fluid flow, and hence is not relevant beyond fracture initiation. Since the theory also neglects the effects of creep, experimental strains before fracture initiation are expected to be higher. A strain profile from a series of gages at several radii and at different flow rates would help to establish the source of the apparent strain amplification.

3.3 EXPLODED CAVITY TESTS

Series 3 - Flow Rate

Hydrofracture tests were performed on unvented exploded cavity spheres of RMG 2C4 to provide comparison data for a parameter study of flow rate. The configuration shown in Figure 2.4 was used in these tests. The 3/8-gram charge shown in Figure 2.5 was the explosive source. An external pressure of 1000 psi (6.895 MPa) was applied to each sphere, and the hydrofracture fluid was dyed water.

Figure 3.4 shows pressure-time hydrofracture records from tests 227, 229, 232, and 249, in which the flow rate was 40.8 cm^3/min, and from tests 244, 245, 248, and 254, in which the flow rate was 122.4 cm^3/min. The major effect of the higher flow rate was to reduce the average time required for fracture initiation from 5.5 to 2.0 seconds. Fracture initiation pressures were comparable for the two groups of tests, and they ranged from 5200 psi (35.85 MPa) to 6800 psi (46.88 MPa). The pressure records indicate that a relatively constant cavity pressure was sufficient to propagate the fractures. Surface gages showed that the sudden loss of cavity pressure was associated with surface cracking.

One factor that apparently contributed to the range of hydrofracture pressures was the type of fracture surface developed. Figure 3.5 shows that the fracture surface in test 244 was planar. The maximum cavity pressure, 5280 psi (36.40 MPa), is at the low end of the spectrum. Figure 3.6 shows the complex fracture pattern developed in test 245.

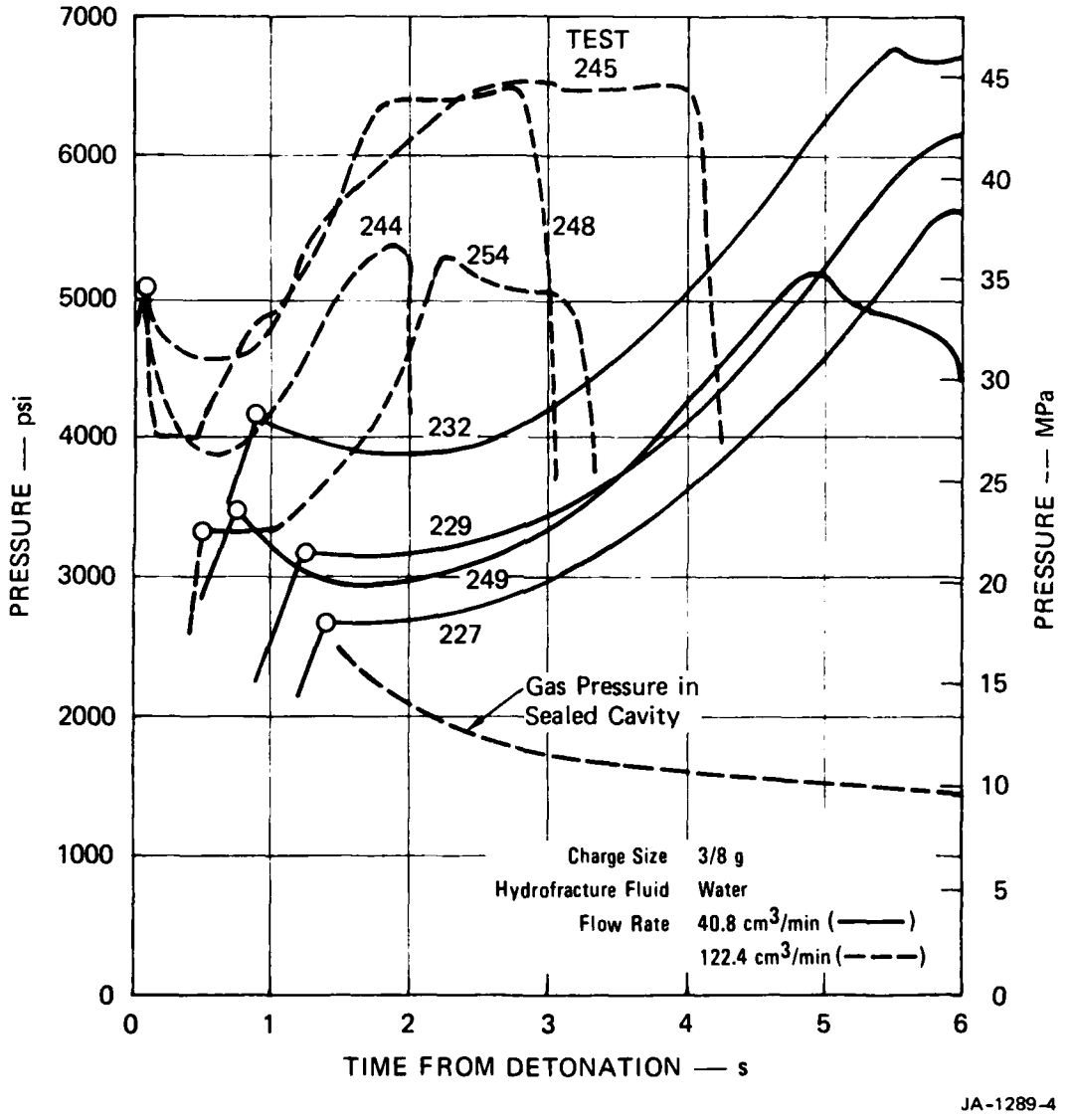

FIGURE 3.4 HYDROFRACTURE PRESSURES FOR UNVENTED EXPLODED CAVITY TESTS – FLOW RATE EFFECT

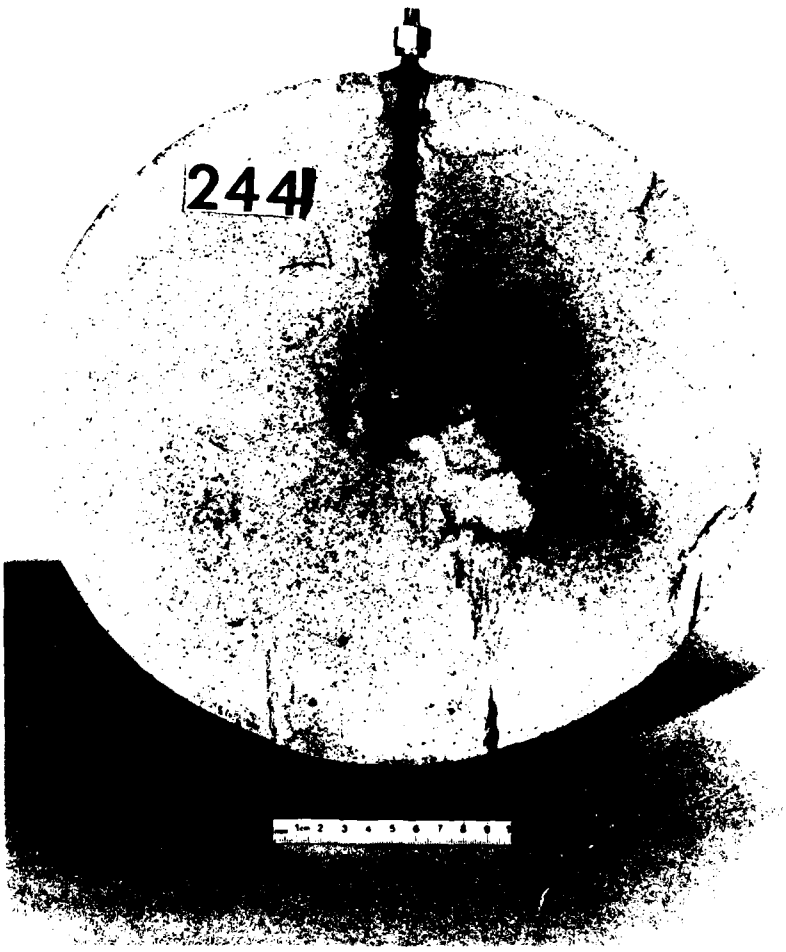

JP-1289-5

FIGURE 3.5 HYDROFRACTURE FROM UNVENTED EXPLODED CAVITY TEST 244 — FLOW RATE EFFECT

JP-1289-6

FIGURE 3.6 HYDROFRACTURE FROM UNVENTED EXPLODED CAVITY TEST 245 — FLOW RATE EFFECT

The maximum cavity pressure in this test, 6400 psi (44.13 MPa), is at the upper end of the spectrum. Figure 3.7 shows the planar fracture in test 249, which gives additional evidence for the connection between relatively low hydrofracture pressures and a planar fracture surface.

In the tests of Figure 3.4, pumping began at the time of charge detonation. However, cavity pressure was not recorded until hydrofracture fluid equilibrated with the cavity gases and the access tube opened. A circle on each curve indicates the instant that the cavity pressure was first measured. Before this time, the pressure transducer recorded the initial prepressure and subsequent pressurization of fluid in the piping above the steel ball (Figure 2.6).

Appendix Figure A.1 shows the TIGER code prediction for the pressure of the detonation products in coupled and uncoupled cavities. For a fully coupled charge, the estimated pressure in an expanded cavity immediately following detonation is 9300 psi (64.12 MPa). Figure 3.4 shows an experimental estimate of the pressure decay curve based on hydrofracture test results. In general, a high fracture initiation pressure is associated with a high minimum cavity pressure. Hence, cavity unloading appears to be an important mechanism in determining the containment capability of an unvented exploded cavity.

Pressure-time hydrofracture records from the previously reported[7] tests 158, 159, 169, and 170, in which the flow rate was 4.26 cm^3/min, are shown in Figure 3.8, along with the records from three of the higher flow rate tests of Figure 3.4 (tests 227, 229, and 232). The low flow rate resulted in an average minimum cavity pressure of 1260 psi (8.69 MPa) and fracture initiation times in excess of 60 seconds. This combination of enhanced cavity unloading and prolonged period of residual stress relaxation resulted in an average fracture initiation pressure of 3000 psi (20.68 MPa), a decrease of 49% from the 5910 psi (40.75 MPa) average for the higher flow rate tests of Figure 3.4.

Figure 3.9 shows that the volume of fluid required to initiate fracture is comparable for different flow rates tested; the cavity volume is 3.6 cm^3. Higher flow rates, however, reduced the volume of fluid required to propagate

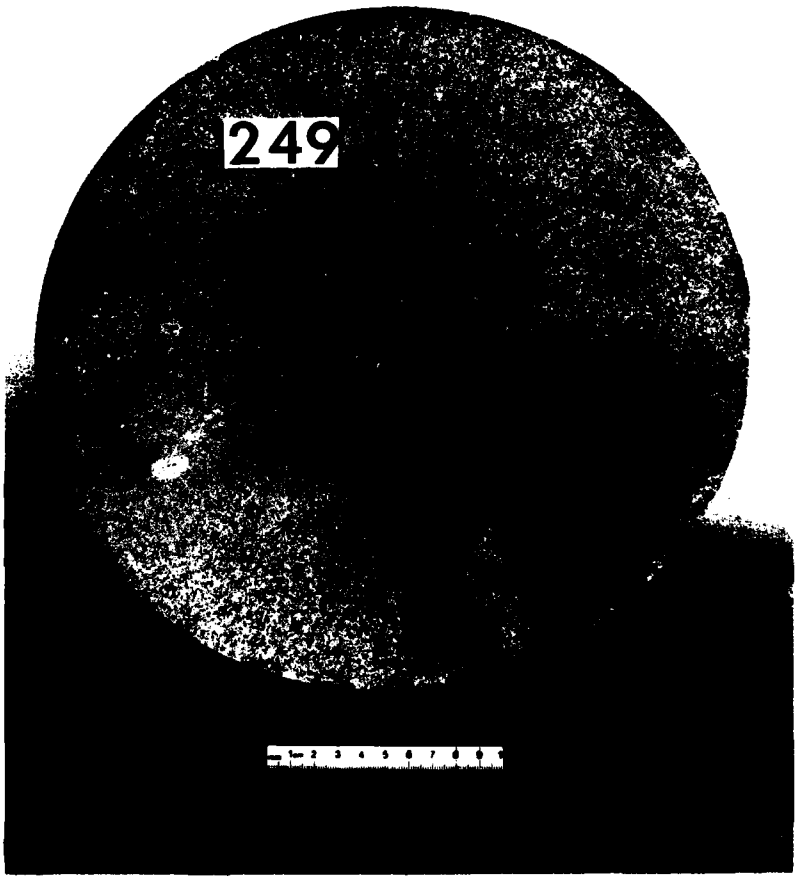

JP-1289-7

FIGURE 3.7 HYDROFRACTURE FROM UNVENTED EXPLODED CAVITY TEST 249 — FLOW RATE EFFECT

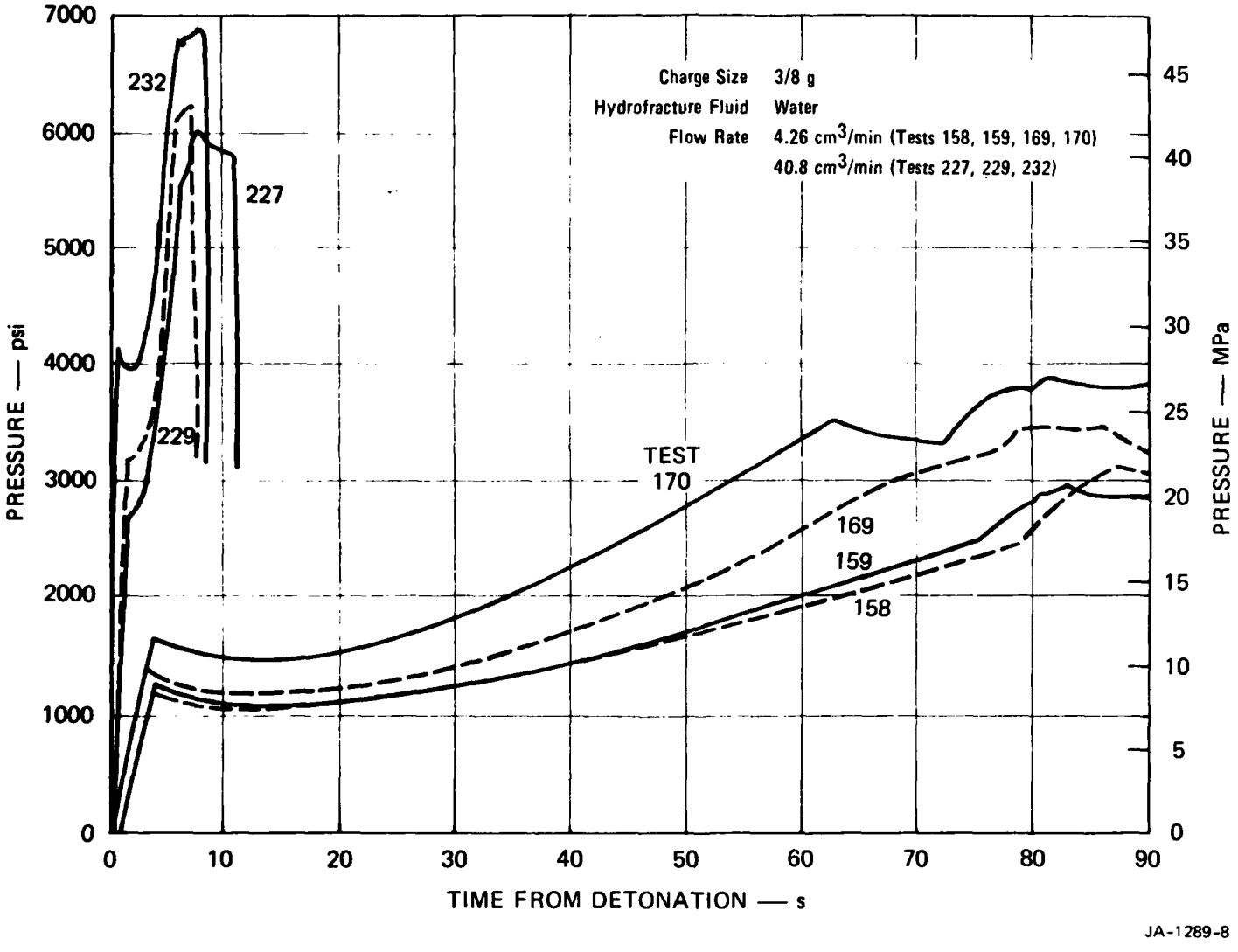

FIGURE 3.8 HYDROFRACTURE PRESSURES FOR UNVENTED EXPLODED CAVITY TESTS 158, 159, 169, 170, 227, 229, AND 232 – PRESSURIZATION RATE EFFECT

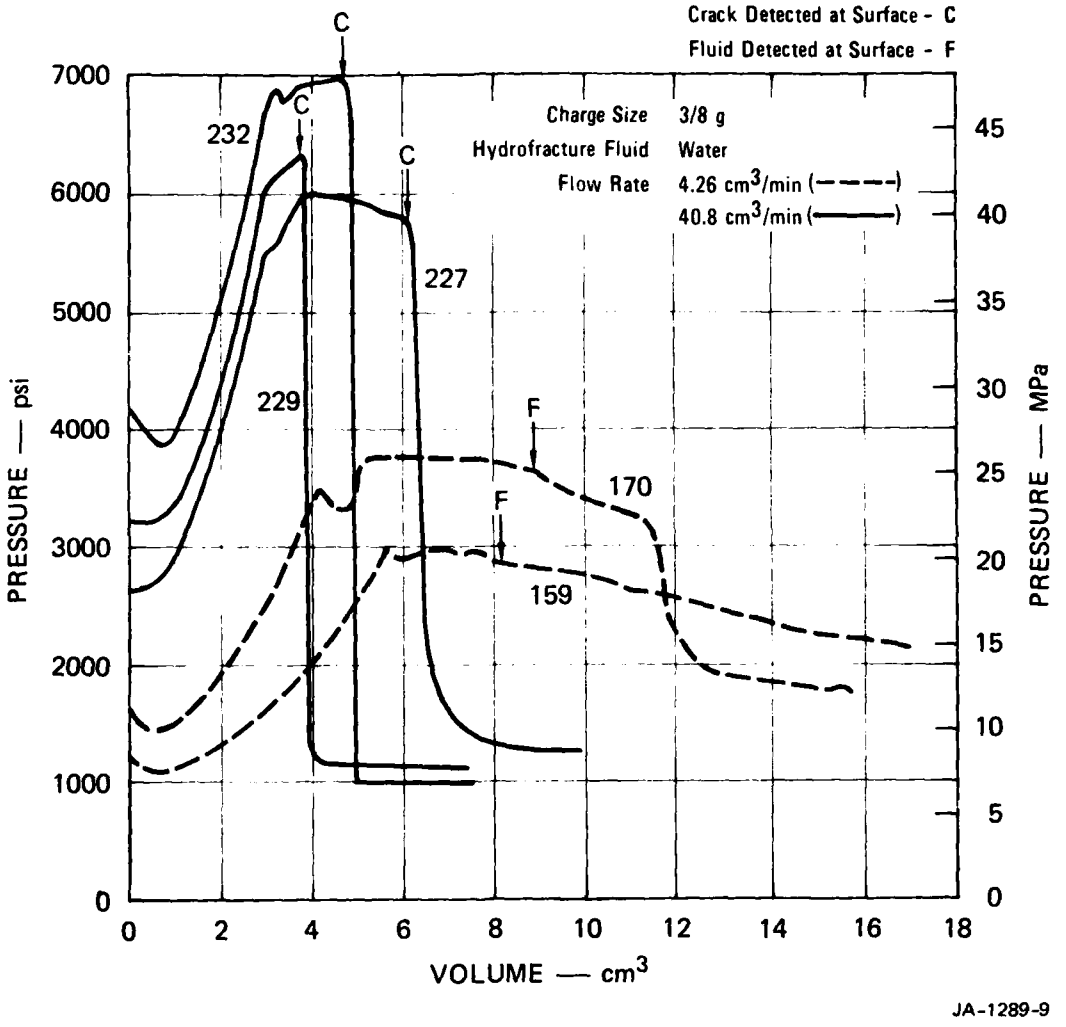

FIGURE 3.9 HYDROFRACTURE PRESSURES FOR UNVENTED EXPLODED CAVITY TESTS 159, 170, 227, 229, AND 232 – FLOW RATE EFFECT

a fracture to the surface, and produced generally wider cracks that resulted in lower steady-state pressures.

Series 4 - Stress Relaxation

Hydrofracture tests 234, 250, and 251 were performed on unvented exploded cavity spheres to separate the effects of cavity unloading and stress relaxation. Figure 3.10 shows the pressure records for these tests in which pumping was stopped and started intermittently in an attempt to maintain a constant cavity pressure following charge detonation. For comparison, the dashed curves show typical pressure records from standard experiments, performed at the same flow rate, but in which there was no period of constant cavity pressure.

The pressure record for test 234 is nearly identical to that of the standard test 232 for the first 4 seconds following charge detonation. Hence, if test 234 had been continued in the standard routine, a fracture initiation pressure of approximately 7000 psi (48.26 MPa) would have been expected. However, 4.8 seconds after charge detonation, pumping was stopped for the first time. The gradual pressure decays in the hydrofracture record represent periods when pumping was stopped. The first two decays are slow and are attributed mainly to system compliance and continued cooling of cavity gases. The third and subsequent decays are faster, indicating loss of fluid from the cavity. Hence, fracture initiation is estimated to occur 13.5 seconds after charge detonation with a cavity pressure of 5650 psi (38.96 MPa). The reduction of fracture initiation pressure from the expected value of 7000 psi (48.26 MPa) for standard testing to 5650 psi (38.96 MPa) in test 234 is a measure of residual stress relaxation.

The pressure records for tests 250 and 251 are similar to those of the standard tests 232 and 249 for the first 3 seconds following charge detonation. In tests 250 and 251, pumping was stopped immediately after a minimum cavity pressure was attained. Attempts were then made to maintain this pressure for 10 seconds by means of intermittent pumping, and then pumping was resumed at a constant flow rate. The effect of this extended period of stress relaxation was to reduce the average fracture initiation pressure from 5950 psi (41.02 MPa) to 4200 psi (28.96 MPa).

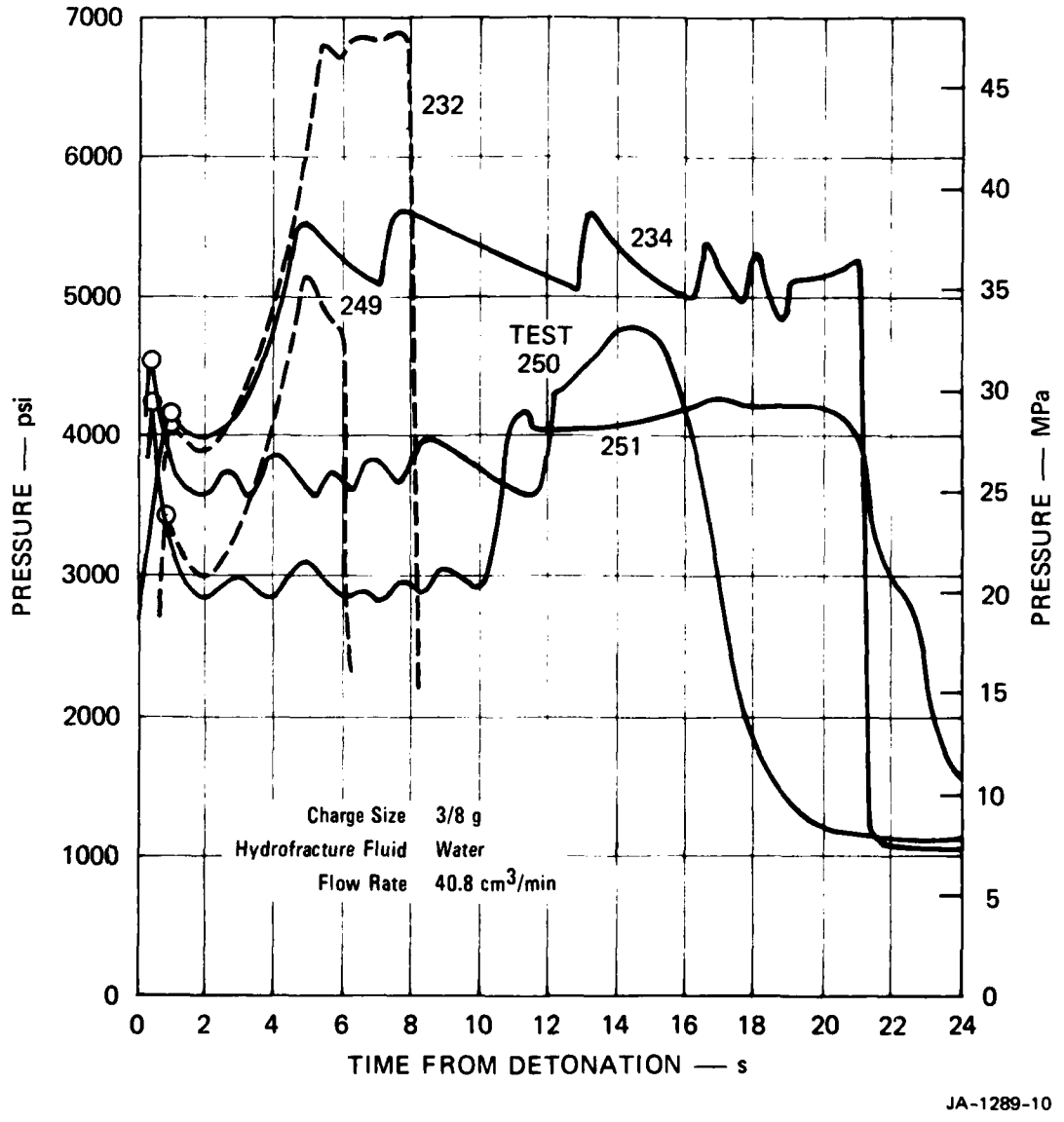

FIGURE 3.10 HYDROFRACTURE PRESSURES FOR UNVENTED EXPLODED CAVITY TESTS – STRESS RELAXATION EFFECT

Series 5 - Uncoupled Cavity

Figure 3.11 shows the pressure records for a series of unvented exploded cavity tests in which the nominal coupling parameters (ratio of initial cavity diameter to charge diameter) were 1 (tests 244, 245, and 248), 1.5 (tests 255 and 256), and 3 (tests 252 and 253). The configuration for uncoupled cavity experiments is shown in Figure 2.8. The charge diameter was 0.404 inch (1.03 cm). The initial cavity diameters were 0.404 inch (1.03 cm), 0.594 inch (1.51 cm), and 1.219 inches (3.10 cm). The corresponding final cavity diameters were 0.808 inch (2.05 cm), 0844 inch (2.14 cm), and 1.312 inches (3.33 cm). Hence, the increases in cavity diameter were 100%, 42%, and 8%, respectively, for the three coupling parameters. The corresponding increases in cavity volume were 3.96, 3.92, and 4.43 cm^3.

Appendix Figure A.2 shows a theoretical estimate of the hydrofracture pressurization curves for the uncoupled cavities tested. The steeper experimental curves indicate that the annular region surrounding the charge was filled with water before charge detonation. Water probably entered the cavity while the hydrofracture system was being filled. The filling technique can be modified easily to retain the annular region of air surrounding the charge by omitting the vacuum step for removing air in the hydraulic line.

Although the tests approximated fully coupled cavity tests, the minimum cavity pressure and corresponding fracture initiation pressure decreased as the coupling parameter increased. The decrease in cavity pressure is attributed to the water available for cooling the detonation products. The decrease in fracture initiation pressure is related to the unloading associated with a reduction in cavity pressure.

The pressure record for test 256 shows an unusual behavior for the first 2 seconds following charge detonation. Relatively constant cavity pressure apparently resulted from gases escaping from the cavity and flowing along the access tube. After the cavity was finally filled with hydrofracture fluid, a typical pressure record was obtained.

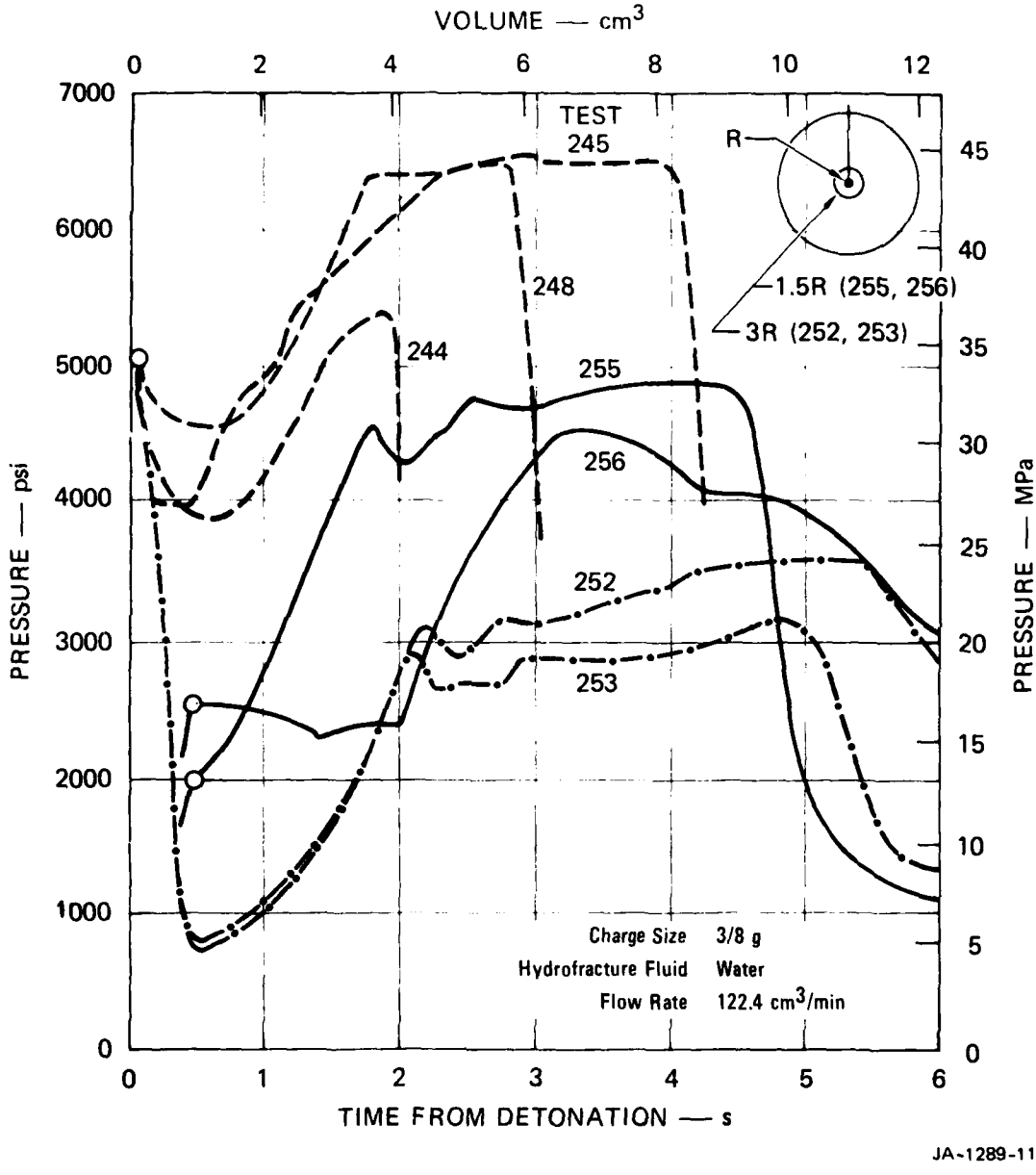

FIGURE 3.11 HYDROFRACTURE PRESSURES FOR UNVENTED EXPLODED CAVITY TESTS – UNCOUPLED CAVITY EFFECT

Series 6 - Vented Cavity

Exploded cavity spheres previously used to test the performance of embedded gages were used to obtain hydrofracture records at higher flow rates for vented cavities. The gage results are described in Series 7 and 8.

Figure 3.12 shows the hydrofracture records for tests 242 and 243. The flow rate was 61.2 cm^3/min, or 14.4 times greater than the 4.26 cm^3/min flow rate for previously reported[7] vented exploded cavity tests. Results of the previous tests are shown as dashed curves in Figure 3.12. In the lower flow rate tests, stress relaxation time between charge detonation and hydrofracture was 20 to 40 minutes. In tests 242 and 243, the corresponding times were 90 minutes and 96 hours, respectively. Fracture initiation pressures for the higher flow rate tests were within the scatter of values of the entire group of tests. The major effect of increased flow rate on containment was to produce initially stable crack growth. In test 242, crack growth stability allowed the cavity pressure to reach a maximum of 3000 psi (20.684 MPa). In test 243, the maximum pressure was 4380 psi (30.199 MPa).

Figure 3.13 shows the complex fracture pattern developed during test 243. As was the case for unvented exploded cavity spheres, high hydrofracture pressures are associated with complex fracture surfaces in vented exploded cavity spheres.

Figure 3.14 shows the pressure-time record for gasfracture test 246 performed on a vented exploded cavity sphere. Nitrogen flowed into the cavity from a high pressure reservoir. The rate of pressurization was equivalent to that developed during a hydrofracture test in which the flow rate was 61.2 cm /min. Pressure-time records for such hydrofracture tests are shown in Figure 3.14 for comparison. Since the gasfracture was performed 5 days after charge detonation, much more relaxation time had occurred than in the hydrofracture tests. This increased relaxation time may be the reason for the 1870 psi (12.89 MPa) fracture initiation pressure being less than the 2380 psi (16.41 MPa) average for the hydrofracture tests, and being comparable to the 1860 psi (12.82 MPa) average for the

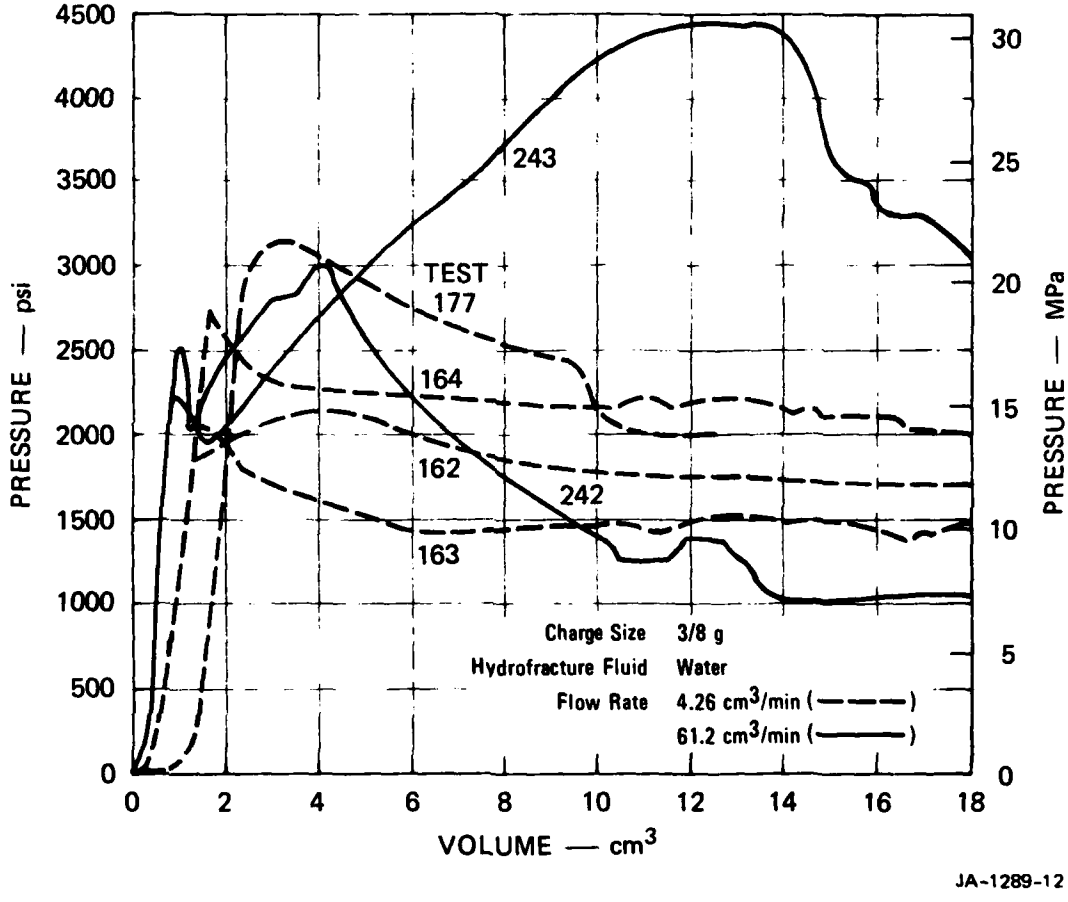

FIGURE 3.12 HYDROFRACTURE PRESSURES FOR VENTED EXPLODED CAVITY TESTS 162, 163, 164, 177, 242, AND 243 – FLOW RATE EFFECT

JP-1289-13

FIGURE 3.13 HYDROFRACTURE FROM VENTED EXPLODED CAVITY
TEST 243 — FLOW RATE EFFECT

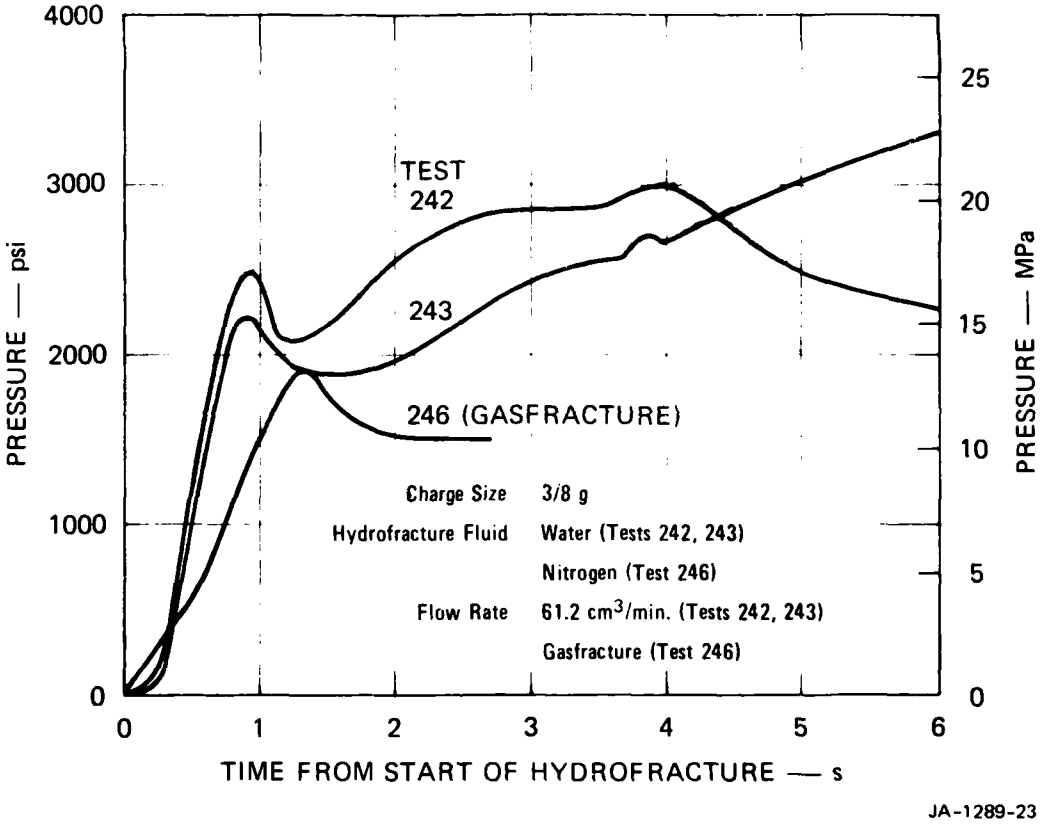

FIGURE 3.14 GASFRACTURE AND HYDROFRACTURE PRESSURES FOR VENTED EXPLODED CAVITY TESTS 242, 243, AND 246

unexploded cavity tests of Series 1. The unstable crack growth following fracture initiation in the gasfracture tests is also characteristic of unexploded cavity tests. Further tests on exploded cavity spheres would be required to separate the effects of gasfracture and stress relaxation.

Series 7 - Strain Measurements

Strain gage packages described in Section 2.3 were embedded in unvented exploded cavity spheres to monitor residual strain decay following charge detonation. The Castall-encapsulated elements were positioned 1.75 inches (4.44 cm) from the center of the charge and were oriented to measure radial and circumferential strains. Figure 2.14(b) shows that this radial position corresponds to an inelastic region in the RMG sphere during the outward propagation of the pulse from the charge. The Castall remains elastic, however, and thus represents an inclusion that affects the initial level of residual strain in the gage. The subsequent strain decay is in an elastic inclusion in grout that is probably behaving viscoelastically.

Figure 3.15 shows the results for tests 250 and 251. The corresponding pressure records are shown in Figure 3.10. In each test, initial strains were measured 500 μseconds following charge detonation. The Castall average initial radial strain was 1240 μstrain compressive, and the average initial circumferential strain was 840 μstrain tensile. In test 250, each strain component decayed 30% during the first 9 seconds following charge detonation. For the corresponding period in test 251, the circumferential strain again decayed 30%, but the radial strain decayed 50%. Since cavity pressure was relatively constant during the strain measurements, the strain decays are attributed to relaxation of the residual stress field.

Figure 3.16 shows the results for test 243. The cavity remained sealed during the test, and only the radial component of strain was measured. The initial radial strain was 2310 μstrain compressive, and decayed 48% during the first 9 seconds and 74% during the first 287 seconds following charge detonation. Since the strain gage responds to cavity gas

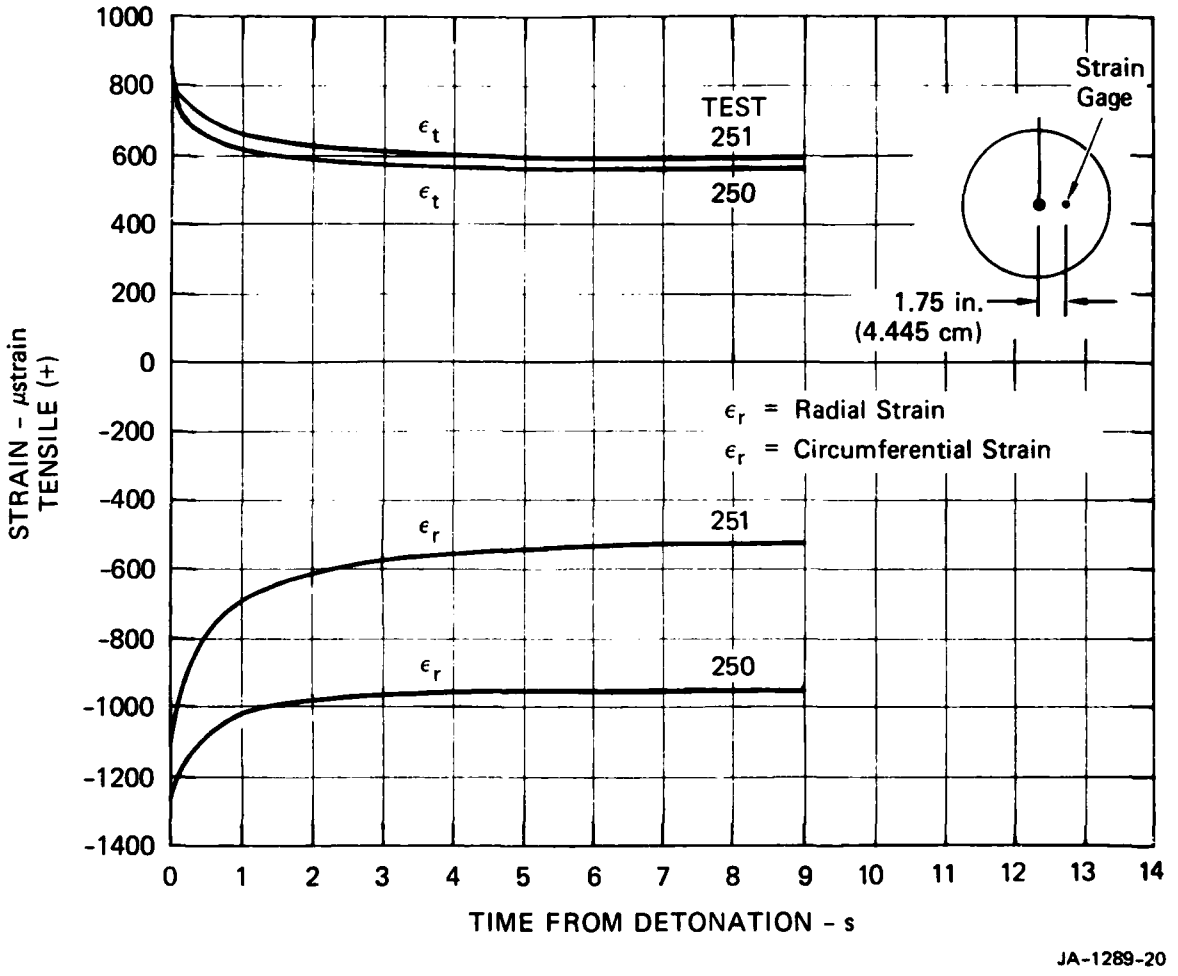

FIGURE 3.15 RESIDUAL RADIAL AND CIRCUMFERENTIAL STRAIN FOR UNVENTED EXPLODED CAVITY TESTS 250 AND 251

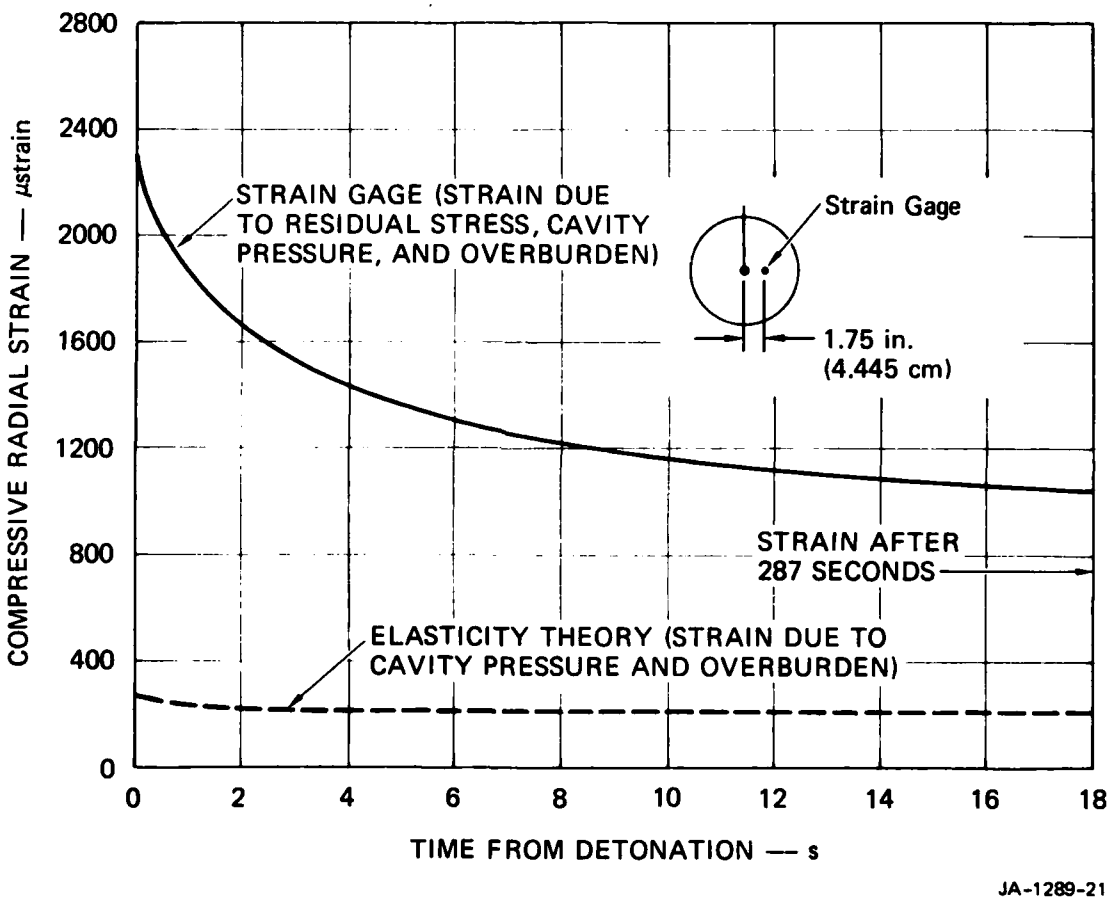

FIGURE 3.16 RESIDUAL RADIAL STRAIN FOR EXPLODED CAVITY TEST 243

pressure and overburden as well as to residual stress, the strain associated with cavity pressure decay and overburden was calculated from elasticity theory, and is shown separately in Figure 3.16. The residual strain decay in test 243 is predominantly attributable to residual stress relaxation.

Series 8 - Stress Measurements

Relaxation of the residual stress field surrounding an exploded cavity may be monitored directly by means of embedded stress gages. Hence, preliminary investigations were performed to establish the suitability of such measurements by means of piezoresistive and flat jack sensing elements.

Ytterbium stress gages were cast in three unvented exploded cavity spheres (tests 243, 246, and 247) to monitor residual stress formation and decay 1.25 inches (3.18 cm) from the center of charge detonation. The gages were oriented to monitor the radial component of stress. Excessive noise from the exploding bridgewire (EBW) detonation obscured the measurement of initial residual stress in test 243. However, residual stress relaxation measurements were made during the first 105 seconds following charge detonation. A 6425-psi (44.299-MPa) decay in compressive radial stress occurred during the first 50 seconds and was followed by negligible decay during the remaining 55 seconds.

The explosive charges in tests 246 and 247 were each detonated by a strand of 1 grain/foot MDF to reduce electrical noise. The gages responded to the stress wave generated by the explosive and indicated a peak stress of approximately 1 kbar. However, the subsequent response of each gage indicated continued straining of the ytterbium element.

The gage package did not generally provide satisfactory residual stress measurements; hence, a modified design incorporating a fully welded package will be developed. The fully welded design has proved reliable in a larger scale version.

A flat-jack gage was positioned to measure radial stress 1.25 inches (3.18 cm) from the center of an unvented cavity. This radial position is

in a region of significant plastic deformation. As expected, charge detonation resulted in closure of the initial gap between the gage plates. However, the plates later began to separate before internal pressure was applied. This response requires further experimentation to resolve. An internal pressure of 1600 psi (11.03 MPa) was applied 55 seconds after charge detonation to return the gage to the pretest configuration. No further changes in gage response were observed during the subsequent 30 minutes. The absence of significant stress decay after 55 seconds is consistent with results from the ytterbium and strain gage tests.

Appendix A

THEORETICAL COOLING AND PRESSURIZATION OF GASES IN UNVENTED EXPLODED CAVITY HYDROFRACTURE TESTS

Theoretical estimates of the cavity pressure in coupled and uncoupled exploded cavities during hydrofracture are presented here as an aid to interpreting the pressure records. The initial cavity pressure immediately following charge detonation was obtained from the SRI TIGER code. Subsequent values were estimated from a thermodynamic analysis governing the equilibrium pressure between cooling cavity gases and compressed hydrofracture fluid.

Figure A.1 shows the pressure of expanding detonation products in a fully coupled cavity and in uncoupled cavities with coupling parameters of 1.5 and 3. These curves were plotted from the data in Tables A.1 through A.3. Since the calculations considered an isentropic expansion and neglected work done in expanding the cavity, the pressures represent upper-bound estimates of the actual cavity pressure.

For the fully coupled cavity, the initial radius r_o is the charge radius (0.51 cm). The initial specific volume (0.9280 cm^3/g) is the value for the PETN/Lucite mixture constituting the charge. The fully expanded cavity radius is 2 r_o = 1.02 cm, and the specific volume of the detonation products is 7.4042 cm^3/g. The corresponding pressure and temperature according to the BKW equation of state are 9300 psi (630 atm) and 999 K, respectively.

For the uncoupled cavity with a coupling parameter of 1.5, the initial radius r_o = 0.71 cm, and the fully expanded cavity radius is 1.51 r_o = 1.07 cm. The pressure and temperature in the fully expanded cavity according to the BKW equation of state are 11,900 psi (850 atm) and 1318 K, respectively.

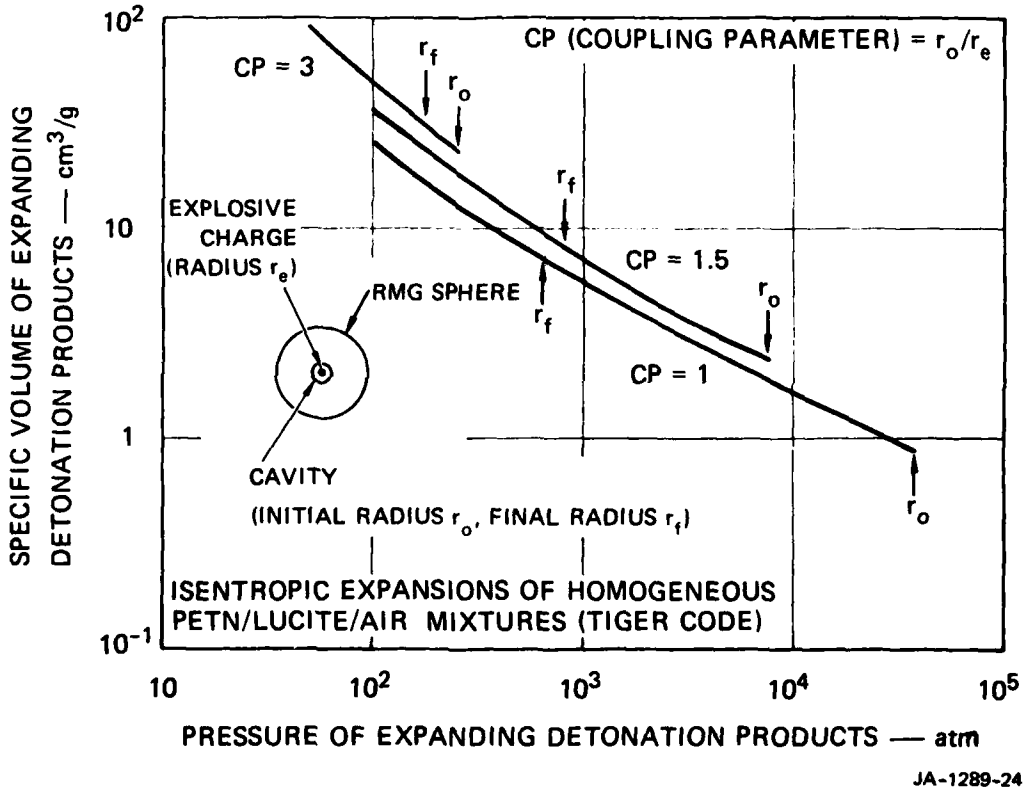

FIGURE A.1 PRESSURE OF EXPANDING DETONATION PRODUCTS IN COUPLED AND UNCOUPLED CAVITIES

Table A.1

PRESSURE AND TEMPERATURE OF EXPANDING DETONATION PRODUCTS[a]
IN A FULLY COUPLED CAVITY

Pressure		Temperature	Specific Volume	Radius Ratio[b]
atm x 10^2	psi x 10^3	(K)	(cm^3/gram)	(r/r_o)
371.0	545.2	1679	0.9280	1.00
205.3	301.7	1636	1.2381	1.10
113.6	167.0	1471	1.5999	1.20
62.9	92.4	1336	2.1026	1.31
34.8	51.2	1226	2.8118	1.45
19.3	28.3	1136	3.8319	1.60
10.7	15.7	1060	5.3336	1.79
6.3	9.3	999	7.4042	2.00[c]
5.9	8.7	993	7.6014	2.02
3.3	4.8	933	11.1153	2.29
1.8	2.7	878	16.6898	2.62
1.0	1.5	825	25.7017	3.03

[a]Pressure-temperature-volume data for PETN/LUCITE mixture from SRI TIGER code (PETN density 1 gram/cm^3, BKW equation of state).

[b]Initial cavity radius r_o = 0.202 in. (0.51 cm).

[c]Final cavity radius ratio (interpolated).

Table A.2

PRESSURE AND TEMPERATURE OF EXPANDING DETONATION PRODUCTS[a] IN AN UNCOUPLED CAVITY WITH COUPLING PARAMETER OF 1.5

Pressure		Temperature (K)	Specific Volume (cm^3/gram)	Radius Ratio[b] (r/r_o)
atm x 10^2	psi x 10^3			
72.8	107.0	1793	2.4410	1.00
47.4	69.7	1668	3.0349	1.08
30.9	45.4	1562	3.8086	1.16
20.1	29.6	1472	4.8308	1.26
13.1	19.2	1394	6.2012	1.36
8.5	12.5	1327	8.0661	1.49
8.1	11.9	1318	8.4340	1.51[c]
5.6	8.2	1267	10.6417	1.63
3.6	5.3	1213	14.2489	1.80
2.4	3.5	1165	19.3646	1.99
1.5	2.3	1120	26.6972	2.22
1.0	1.5	1079	37.2952	2.48

[a]Pressure-temperature-volume data for PETN/LUCITE mixture from SRI TIGER code (PETN density 1 gram/cm^3, BKW equation of state).

[b]Initial cavity radius r_o = 0.279 in. (0.71 cm).

[c]Final cavity radius ratio (interpolated).

Table A.3

PRESSURE AND TEMPERATURE OF EXPANDING DETONATION PRODUCTS[a]
IN AN UNCOUPLED CAVITY WITH COUPLING PARAMETER OF 3

Pressure		Temperature	Specific Volume	Radius Ratio[b]
atm x 10	psi x 10^2	(K)	(cm^3/gram)	(r/r_o)
25.1	36.9	1459	23.2080	1.00
18.2	26.7	1397	30.3666	1.09
17.7	26.0	1392	31.2304	1.10[c]
13.2	19.4	1342	39.8683	1.20
9.5	14.0	1292	52.4524	1.31
6.9	10.2	1247	69.1366	1.44
5.0	7.4	1205	91.2852	1.58
3.6	5.3	1167	120.7214	1.73
2.6	3.9	1131	159.8832	1.90
1.9	2.8	1098	212.0325	2.09
1.4	2.0	1067	281.5362	2.30
1.0	1.5	1039	374.2421	2.53

[a]Pressure-temperature-volume data for PETN/LUCITE/AIR mixture from SRI TIGER code (PETN density 1 gram/cm^3, ideal gas equation of state).

[b]Initial cavity radius r_o = 0.596 in. (1.51 cm).

[c]Final cavity radius ratio (interpolated).

Finally, for the uncoupled cavity with a coupling parameter of 3, the initial radius r_o = 1.51 cm, and the fully expanded cavity radius is 1.10 r_o = 1.66 cm. The pressure and temperature in the fully expanded cavity according to the ideal gas equation of state are 2600 psi (177 atm) and 1392 K, respectively.

Following charge detonation, hydrofracture fluid is pumped at a constant rate and the cavity gas cools. If the cavity remains sealed, fluid pressure increases while gas pressure decays. For a given fluid, the rate of pressure increase is governed by the pumping rate and initial volume. For a fully coupled cavity, an estimate of the gas pressure decay is provided by the experimental cooling curve shown in Figure 3.4. When the cavity finally opens, fluid and gas mix, and a time-varying equilibrium pressure is established. The initial part of unvented exploded cavity hydrofracture records represent this process.

Representative hydrofracture records chosen from the coupled and uncoupled cavity configurations are shown in Figure A.2. Also shown are theoretical estimates for the initial pressurization rate of the hydrofracture fluid and cavity gas mixture. These theoretical curves represent the equilibrium pressure established between the hydrofracture liquid and the cavity gas at any time. For a compressible liquid, the pressure-volume relationship is

$$K_\ell = - \frac{p_{\ell f} - p_{\ell i}}{\frac{V_{\ell f} - V_{\ell i}}{V_{\ell i}}} \qquad (A.1)$$

where K_ℓ = bulk modulus
$p_{\ell i}$ = initial pressure
$p_{\ell f}$ = final pressure
$V_{\ell i}$ = initial volume
$V_{\ell f}$ = final volume

For an ideal gas, the isentropic pressure-volume relationship is

$$p_{gi} V_{gi}^{\gamma} = p_{gf} V_{gf}^{\gamma} \qquad (A.2)$$

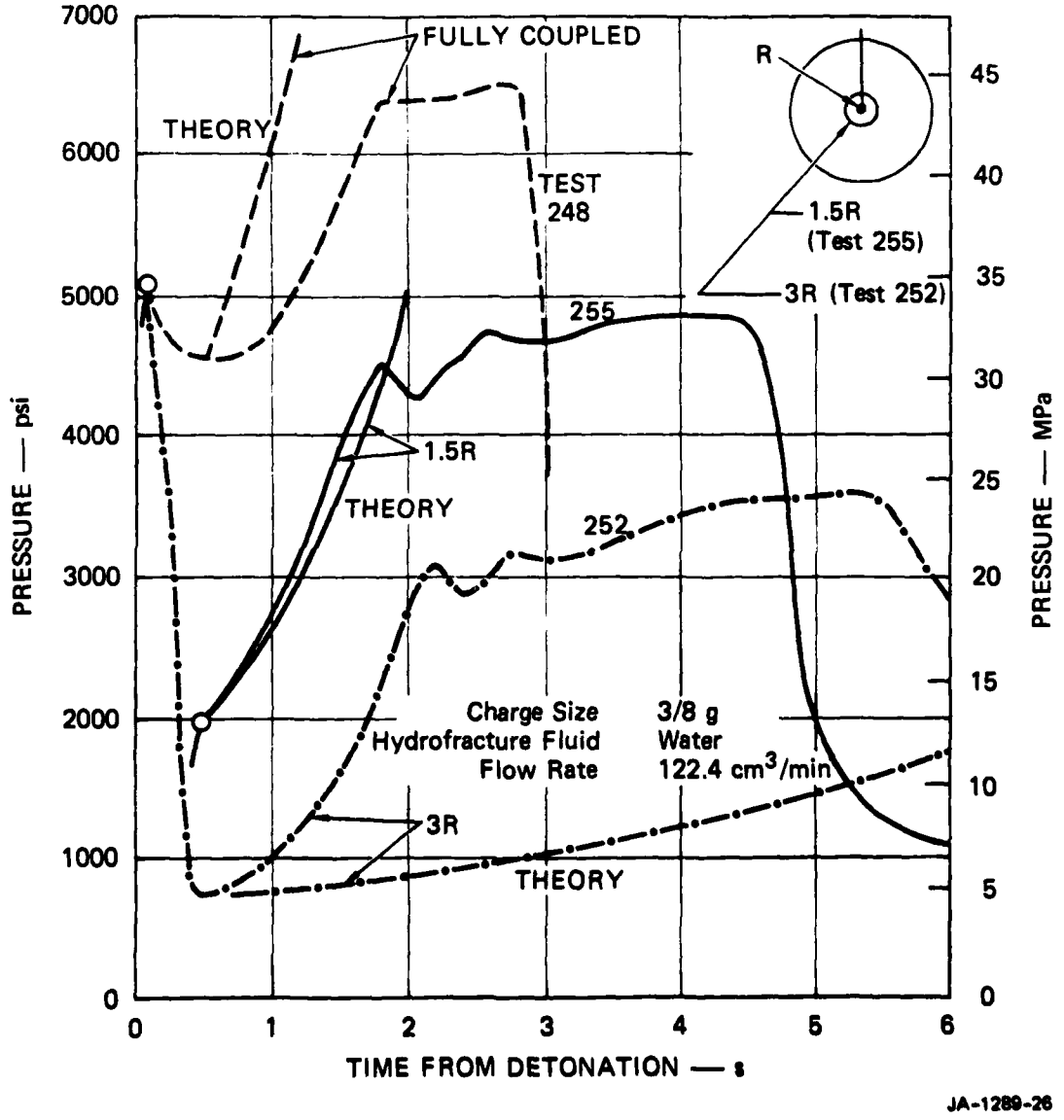

FIGURE A.2 THEORETICAL AND EXPERIMENTAL HYDROFRACTURE PRESSURES FOR UNVENTED EXPLODED CAVITY TESTS - UNCOUPLED CAVITY EFFECT

where p_{gi} = initial pressure
p_{gf} = final pressure
V_{gi} = initial volume
V_{gf} = final volume
γ = ratio of specific heats

Equilibrium requires that

$$p_{\ell f} = p_{gf} \tag{A.3}$$

In addition, the total volume of liquid and gas is fixed at a given time during hydrofracture. Hence

$$(V_{\ell f} - V_{\ell i}) + (V_{gf} - V_{gi}) = 0 \tag{A.4}$$

Substituting equations A.1, A.2, and A.3 into equation A.4 yields the following expression for the liquid-gas equilibrium pressure:

$$(p_{\ell f})^{1+1/\gamma} + (p_{\ell f})^{1/\gamma}\left(\frac{V_{gi}}{V_{\ell i}} K_\ell - p_{\ell i}\right) - \frac{V_{gi}}{V_{\ell i}} K_\ell (p_{gi})^{1/\gamma} = 0 \tag{A.5}$$

For the fully coupled configuration, p_{gi} is taken from the experimental cooling curve. For the uncoupled cavities, p_{gi} is estimated from the ideal gas relation $p_{gi} V_{gi}^{\gamma}$ = constant, where $\gamma = 1.4$ and the constant is determined from the coupled cavity data. From calibration of the hydrofracture system, $p_{\ell i} = 10{,}000$ psi/s (t), where t is the time from detonation. In Equation A.5, γ was chosen to be 1.4 and the equation was solved numerically.

Figure A.2 shows that the theory predicts the rate of pressurization in a fully coupled cavity. For the uncoupled cavities, however, the theoretical rates of pressurization range from slightly less than to much less than the corresponding experimental rates. The discrepancy can be resolved by considering the cavities to be fluid-filled before charge detonation.

Appendix B

MATERIAL PROPERTIES

Presented here are material properties of the rock-matching grout RMG 2C4 and the epoxy Castall that are relevant to the current investigations. Additional strength properties of 2C4 are described in previous reports.[5-7]

Table B.1 provides the mixture and heat curing cycle for the rock-matching grout. Table B.2 summarizes the commonly used physical and mechanical properties of 2C4 and Castall.

The scatter in unconfined crush strength and tensile strength associated with the testing of a large number of standard 2-inch-diameter (5.08-cm) cylinders of 2C4 is shown in Figures B.1 and B.2. These figures show that, in general, reasonable tolerance is maintained on material strength.

A separate study was conducted to determine the effect of curing temperature and age on the crush strength of the grout. One group of standard cylinders was subjected to the normal heat bath cure described in Table B.1. A second group was cured in room temperature (25°C) water. Samples from each batch were tested periodically as shown in Figure B.3. The average strength for each group showed a general increase with age. The effect of the heat bath was to reduce the overall scatter and provide a consistently stronger grout.

Table B.1

MIXTURE[a] FOR ROCK-MATCHING GROUT RMG 2C4

Component	Percent of RMG 2C4 Mixture
Type I-II Portland cement	32.691
Sand (20-40 Monterey)	21.896
Barite (barium sulfate)	20.848
Bentonite (gel)	2.837
CFR 2 (concrete friction reducing compound)	0.078
Water	21.650

[a]Curing procedure: sealed in plastic and submerged in water with the following temperature sequence: raise to 54°C over 48-hour period, hold at 54°C for 48 hours, lower to 25°C over 36-hour period.

Table B.2

PROPERTIES OF ROCK-MATCHING GROUT RMG 2C4 AND CASTALL

(a) PHYSICAL PROPERTIES

Physical Property	RMG 2C4	Castall
Density (g/cm^3)		
Aged	2.15	2.20
Dry	1.75	
Grain	2.87	
Water by wet weight (%)	18.6	
Porosity (%)	39	
Saturation (%)	100	
Air voids (%)	0	
Longitudinal velocity (km/s)	3.29	2.98
Shear velocity (km/s)	1.82	1.70
Modulus in compression (psi)	2.64×10^6	2.32×10^6
Shear modulus (psi)	1.03×10^6	9.22×10^5
Bulk modulus (psi)	2.00×10^6	1.60×10^6
Poisson's ratio	0.28	0.26
Permeability (μd)	3.0	

(b) MECHANICAL PROPERTIES

Material	Average Strain Rate (s^{-1})	Compressive Strength (psi)	Tensile Strength (psi)
RMG 2C4	Static	3940	530
RMG 2C4	0.15	5330	900

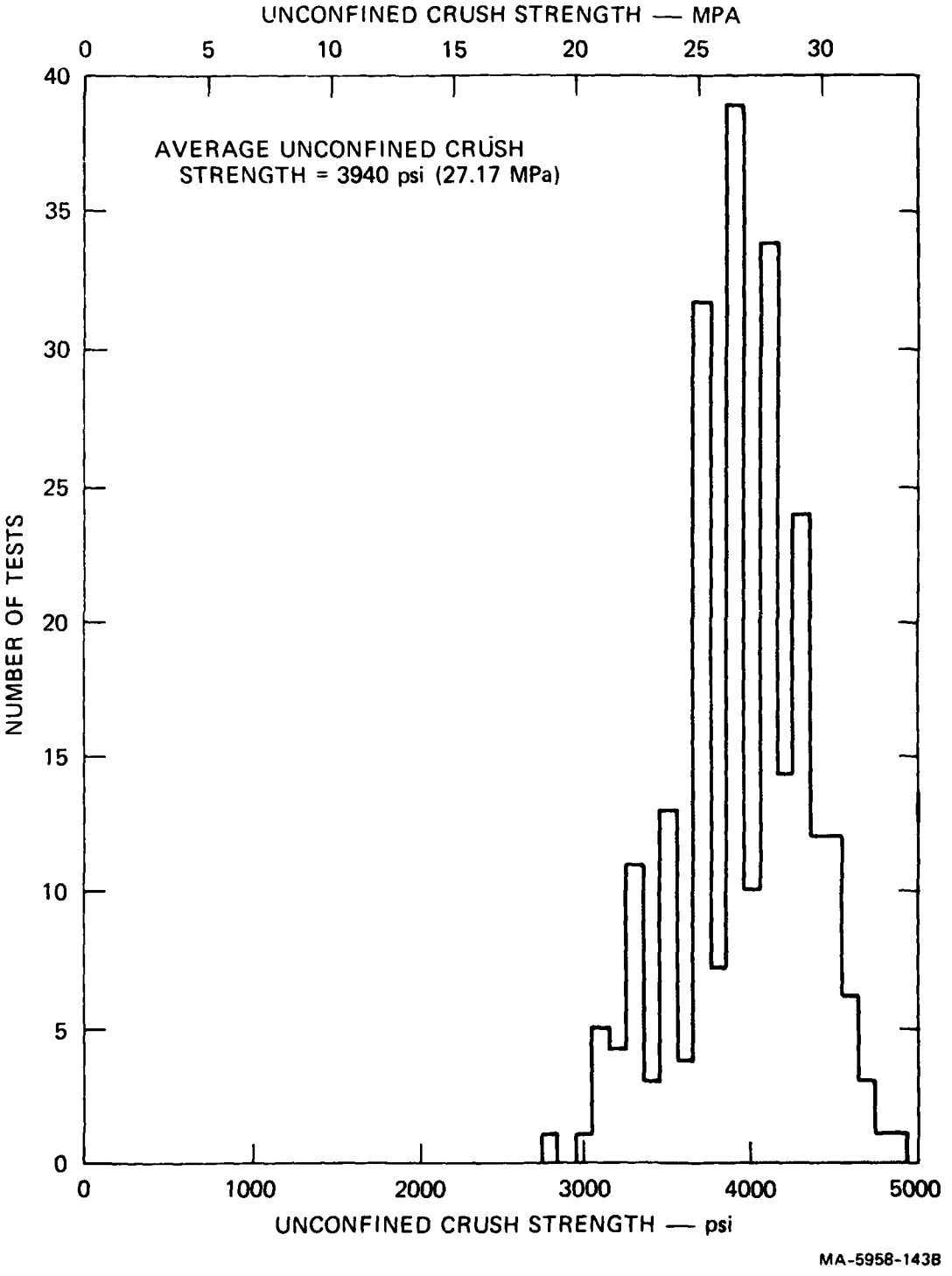

FIGURE B.1 UNCONFINED CRUSH STRENGTH OF ROCK-MATCHING GROUT RMG 2C4

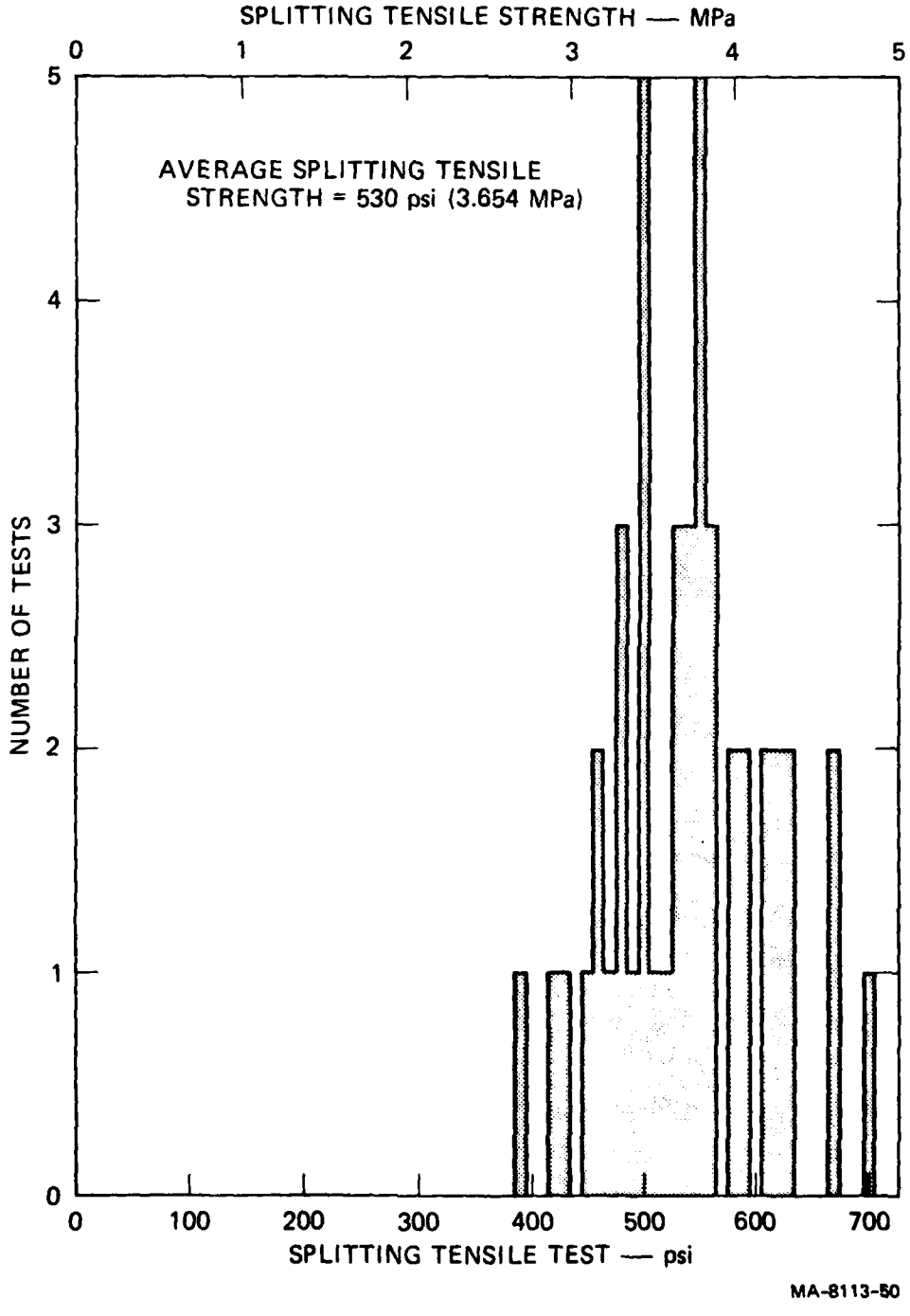

FIGURE B.2 SPLITTING TENSILE STRENGTH OF ROCK-MATCHING GROUT RMG 2C4

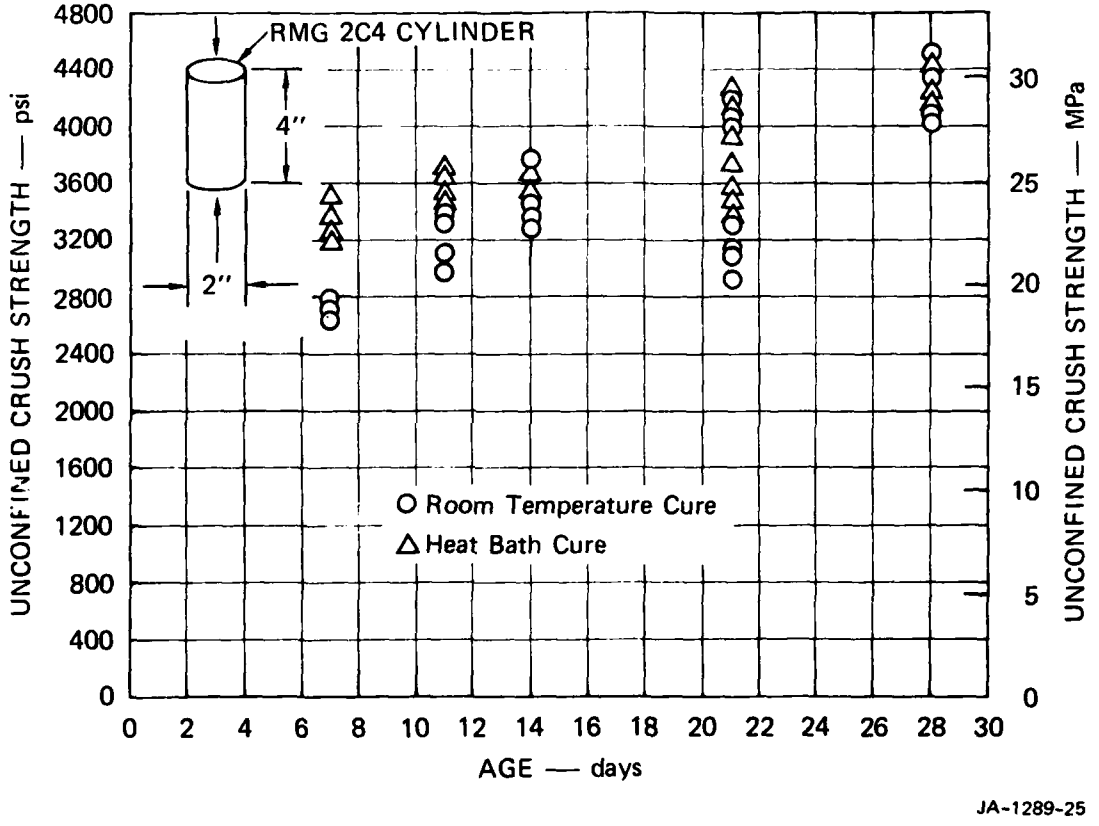

FIGURE B.3 EFFECTS OF CURING TEMPERATURE AND AGE ON THE UNCONFINED CRUSH STRENGTH OF ROCK-MATCHING GROUT RMG 2C4

REFERENCES

1. R. W. Gates and C. F. Petersen, "A Laboratory Method for Studying Stemming of Line-of-Sight Tunnels in Underground Nuclear Tests," SRI Final Report DNA 3058Z, Contract DNA001-72-C-0047 (November 1972).

2. R. W. Gates, C. F. Petersen, and A. L. Florence, "Laboratory Method for Studying Stemming of Line-of-Sight Tunnels in Underground Nuclear Tests," SRI Final Report DNA 3592F, Contract DNA001-73-C-0122 (December 1973).

3. A. L. Florence, "Laboratory Investigation of Stemming of Horizontal Line-of-Sight (HLOS) Underground Nuclear Tests," SRI Final Report DNA 3684F, Contract DNA001-74-C-0101 (February 1975).

4. A. L. Florence, "Laboratory Investigation of Stemming and Containment in Underground Nuclear Tests," SRI Final Report DNA 4149F, Contract DNA001-75-C-0083 (October 1976).

5. J. C. Cizek and A. L. Florence, "Laboratory Investigation of Containment in Underground Nuclear Tests," SRI Final Report DNA 4846F, Contract DNA001-77-C-0025 (January 1978).

6. J. C. Cizek and A. L. Florence, "Laboratory Studies of Containment in Underground Nuclear Tests," SRI Final Report DNA 4847F, Contract DNA001-77-C-0025 (January 1979).

7. J. C. Cizek and A. L. Florence, "Laboratory Studies of Containment in Underground Nuclear Tests," Draft Final Report, Contract DNA001-79-C-0094 (January 1980).

8. A. L. Florence and T. C. Kennedy, "A Simple Analysis for Containment Studies," SRI Topical Report 76-3702-2, Contract DNA001-75-C-0083 (August 1976).

9. L. Seaman, "SRI PUFF 3 Computer Code for Stress Wave Propagation," prepared for Air Force Weapons Laboratory, Air Force Systems Command, Kirtland AFB, New Mexico, Technical Report No. AFWL-TR-70-51, SRI International, Menlo Park, California (September 1970).

10. N. Rimer and K. Kie, "Spherically Symmetric Numerical Simulation of the SRI Grout Spheres Containment Experiments," Systems, Science and Software Topical Report SSS-R-79-3831, Contract DNA001-77-C-0099 (October 1978).

11. J. C. Cizek, A. L. Florence, and D. D. Keough, "Effects of Faults on Spherical Wave Propagation," SRI Quarterly Progress Report No. 2, Contract DNA001-80-C-0287 (November 1980).

DISTRIBUTION LIST

DEPARTMENT OF DEFENSE

Defense Nuclear Agency
ATTN: SPTD, T. Kennedy
4 cy ATTN: TITL

Defense Technical Information Center
12 cy ATTN: DD

Field Command
Defense Nuclear Agency
ATTN: FCTT, W. Summa
3 cy ATTN: FCTK, C. Keller

Field Command Test Directorate
Test Construction Division
Defense Nuclear Agency
ATTN: FCTC, J. Lacomb

DEPARTMENT OF ENERGY

Department of Energy
Nevada Operations Office
ATTN: R. Newman

OTHER GOVERNMENT AGENCY

Department of the Interior
U.S. Geological Survey
ATTN: R. Carroll

DEPARTMENT OF ENERGY CONTRACTORS

Lawrence Livermore National Lab
ATTN: B. Hudson
ATTN: J. Shearer
ATTN: R. Terhune
ATTN: D. Oakley

Sandia National Lab
ATTN: C. Mehl
ATTN: C. Smith
ATTN: R. Bass

DEPARTMENT OF ENERGY CONTRACTORS (Continued)

Los Alamos National Laboratory
ATTN: S. Schmidt
ATTN: G-6, E. Jones
ATTN: R. Brownlee
ATTN: F. App
ATTN: L. Germain
ATTN: A. Davis

DEPARTMENT OF DEFENSE CONTRACTORS

California Research & Technology, Inc
ATTN: M. Rosenblatt

Kaman Tempo
ATTN: DASIAC

Pacific-Sierra Research Corp
ATTN: H. Brode

Pacifica Technology
ATTN: G. Kent

Physics International Co
ATTN: E. Moore

R & D Associates
ATTN: P. Haas

SRI International
ATTN: A. Florence

Systems, Science & Software, Inc
ATTN: R. Duff

Terra Tek
ATTN: S. Green


DAT
ILM